Neutral particle effect on plasma detachment and characterization of ion behavior in the end region of GAMMA 10/PDX

Kunpei Nojiri

February 2019

Neutral particle effect on plasma detachment and characterization of ion behavior in the end region of GAMMA 10/PDX

Kunpei Nojiri
Doctoral Program in Physics

Submitted to the Graduate School of
Pure and Applied Sciences
in Partial Fulfillment of the Requirements
for the Degree of Doctor of Philosophy in
Science

at the
University of Tsukuba

Contents

Chapter 1

Introduction

1.1 Heat and particle handling in magnetic confinement fusion

Enormous researches have contributed to realize the magnetic confinement fusion reactor. At the present stage, tokamak is the most promising plasma confinement type and the International Thermonuclear Experimental Reactor (ITER) [1] is also a tokamak type. In recent tokamaks, divertor configuration [2] is adopted and it will also be adopted to ITER and DEMO reactors [3, 4]. Figure 1.1.1 shows schematics of poloidal cross section of a tokamak with the divertor configuration. In the configuration, particles escaping from the core region are transported to the divertor region through scrape-off layer (SOL). This configuration reduces core plasma dilution with particles resulting from plasma-wall interaction (PWI) and pumps helium ash resulting from nuclear fusion reaction. Although the divertor configuration improves the core plasma performance of tokamaks as reviewed in Ref. [2], the divertor plate suffers heat and particle loads since the loads are concentrated at the plate. In ITER, while the engineering limits of the heat flux density at the divertor plate with copper (CuCrZr) alloy cooling tubes are estimated to be 10 MW m^{-2} for the steady state and 20 MW m^{-2} for transient events (up to 10 s), heat flux density in the SOL is expected to be ~1 GW m^{-2} [5] and heat flux density onto the divertor plate will easily exceed the engineering limit if significant reduction measures were not taken. In DEMO, while the heat flux entering the SOL is expected to be two or three times larger than that in ITER, the engineering limit at the divertor plate with CuCrZr cooling tubes is the same 10 MW m^{-2} and moreover, it will be 5 MW m^{-2} if the cooling tubes are made from reduced activation ferritic/martensitic (RAFM) steel [4]. If the heat load on the divertor plate exceed the tolerable value, melting of the material will occur and the reactor will be seriously damaged. Therefore,

reduction of the loads on the divertor plate is one of crucial issues to realize the nuclear fusion reactor. In order to reduce the heat load, plasma detachment (or divertor detachment) is considered to be an effective method as introduced in the next section.

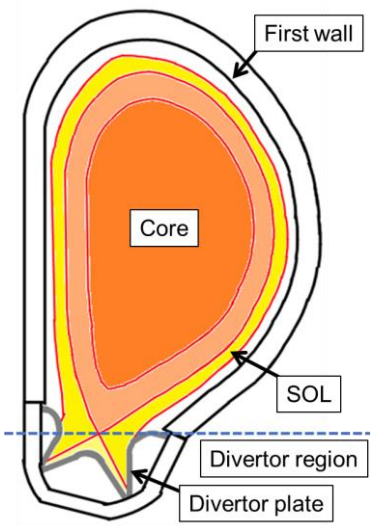

Figure 1.1.1 Schematic of poloidal cross-section of a tokamak with divertor configuration.

1.2 Plasma detachment and plasma-gas interaction

Plasma detachment is considered to be an effective method to reduce the heat and particle loads on the divertor plate. Figure 1.2.1 shows schematic drawings of spatial characteristics of detached plasma. Plasma detachment is a condition where plasma temperature, density and pressure near the target plate are significantly reduced due to plasma-gas interactions including radiation, ionization, charge-exchange and subsequent volumetric recombination. Plasma detachment in tokamaks has been achieved by increase in the neutral density near the target plate by means of increasing the core plasma density or of seeding additional neutral gas [6-10]. In order to reduce the loads on the divertor and to keep the nuclear fusion reaction in the core, it is necessary to realize the low temperature detached plasma with high neutral density in the divertor region and the burning plasma in the core. To achieve good controllability of the detached plasma, it is important to understand the physical mechanism of plasma detachment.

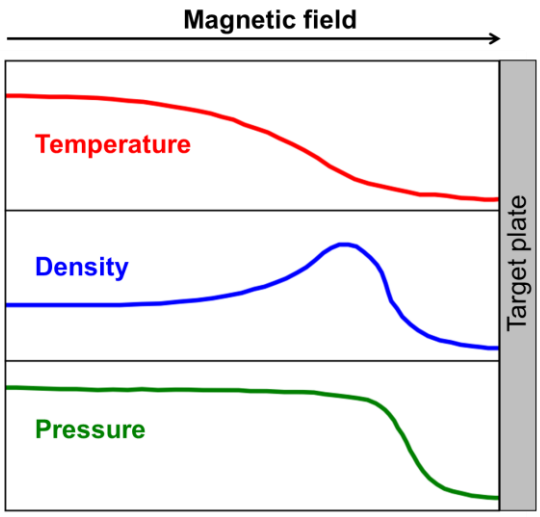

Figure 1.2.1 Schematic drawings of spatial characteristics of detached plasma.

Figure 1.2.2 shows diagram of interactions among ions, electrons and neutral particles including atoms and molecules. The reaction rate of each interaction is written as $n_1 n_2 k$, where n_1 and n_2 are density of particle 1 and 2 and k is the rate coefficient which depends on each particle's temperature and on quantum states of the neutral particle when the interaction is related to the neutral particle. Since plasma detachment is achieved by the complex effect of the interactions

among charged and neutral particles, not only each density but also each temperature of the particles and quantum states of neutral particles as shown in Fig. 1.2.2 are important parameters to understand the mechanism of plasma detachment.

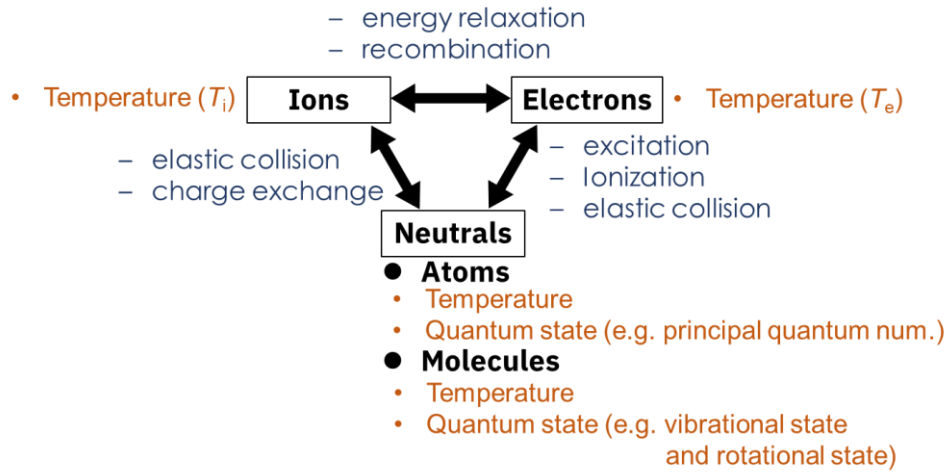

Figure 1.2.2 Diagram of interactions among ions, electrons and neutral particles. Important parameters in addition to each density are also shown.

1.3 Ion temperature measurement in SOL/Divertor

Electron temperature (T_e) and density (n_e) can be measured by Langmuir probe (LP) and Thomson scattering (TS) measurements in SOL/divertor. On the other hand, ion temperature (T_i) is more difficult to be measured. In the detached divertor condition, the measuring results of T_i of SOL plasma are very little and T_i of divertor plasma has not been measured. But in the attached divertor condition, recent measurements have shown that T_i tends to be higher than T_e except for strongly collisional condition [10-11]. Next, some of recent measuring results of T_i in attached divertor condition of relatively large tokamaks are introduced. Most of these measurements were done in SOL (upstream of divertor region) and the MAST spherical tokamak had a T_i diagnostic in the divertor in addition to the SOL. These T_i were measured by the retarding field analyzer (RFA), charge exchange recombination spectroscopy (CXRS) or ion sensitive probe (ISP).

In JET tokamak, T_i profile in the top edge of SOL was measured by the RFA and was compared with T_e profile measured by the LP [12]. Two RFAs are installed in one fast reciprocating drive system which enables the RFAs to move vertically from the upper side of the vacuum vessel [13]. One of the RFAs faces the outer divertor side and the other faces the inner divertor side. The LP is installed in another reciprocating drive system which is mounted at the same location in the poloidal cross-section as the RFAs but displaced 180° toroidally. The experiment was conducted in ohmic phase of low density plasma with $\bar{n}_e$~2×10^{19} m^{-3}. In the range of midplane separatrix distance from ~2.5 mm to ~40 mm, T_e was almost uniform and it was ~20 eV. The both profiles of T_i measured by the RFAs had a gradient. Near the separatrix (the distance ~ 0 mm), T_i was higher than that measured at the outer position. The ion temperature measured by the RFA facing the outer divertor side decreased from ~80 eV to ~30 eV and T_i measured by the other RFA decreased from ~50 eV to ~ 20 eV.

In JT-60U with W shaped divertor, T_i profile in SOL was measured by the CXRS and was compared with T_e profile measured by the LP and the TS system [14]. The view line of the CXRS was about 1 m above the SOL midplane and a charge exchange populated line of C^{5+} was used. The LP was mounted on fast reciprocating drive system at the midplane of SOL [15]. The TS system had view lines near the top of SOL. The experiment was conducted in a L-mode discharge with high density ($\bar{n}_e$ ~2.4×10^{19} m^{-3}) and detached divertor plasmas which were formed by deuterium gas puffing. The T_e profile measured by the TS and LP had a gradient with distance from separatrix. With increase in the distance from ~0 mm to ~60mm, T_e decreased from ~100 eV to ~20 eV. The T_i profile measured by the CXRS also had a gradient. In the same distance range, T_i decreased from ~250 eV to 100 eV.

In DIII-D, T_i profile near the SOL midplane was measured by the CXRS using a C^{6+} line and

was compared with T_e profile measured by the LP and the TS system [16]. The LP is mounted on the reciprocating drive system [17]. In the SOL, T_e was around 20 eV and T_i was around 200 eV.

In Alcator C-Mod, T_i profile near the SOL midplane was measured by the ISP and the CXRS using a B^{5+} line and was compared with T_e profile measured by the TS system and the LPs [18]. The ISP was mounted on the reciprocating system [19]. The CXRS covered the region where the distance from the separatrix ρ = ~15 mm to +2 mm and the ISP covered the region where ρ = ~5 mm to +10 mm. The TS system had view lines near the top edge of SOL. The LPs were installed on the outer divertor plates. The density scan was conducted from $\bar{n}_e = 0.6\times10^{20}$ m^{-3} to $\bar{n}_e = 0.6\times10^{20}$ m^{-3} in ohmic L-mode discharge without auxiliary heating. Through the density scan, all T_e profiles measured by the TS and LP had a gradient with ρ and T_e in the SOL decreased from ~30 eV to ~20 eV with increase in ρ from ~0 mm to ~+10 mm. With increase in $\bar{n}_e$, T_i near the SOL midplane measured by CXRS decreased. Near the separatrix, T_i measured by the CXRS decreased from ~120 eV to ~60 eV with increase in $\bar{n}_e$. The T_i profiles measured by the ISP with relatively low $\bar{n}_e$ agreed with that measured by the CXRS, though those with relatively high $\bar{n}_e$ suggested that those were space charge limited.

In MAST spherical tokamak, the RFAs were installed near the SOL midplane and the outer divertor. Near the midplane, T_i profiles measured by the RFA and the CXRS were compared with T_e profile measured by the TS system. Near the divertor plate, T_i profiles measured by the other RFA were compared with T_e profile measured by the LP mounted on the plate. These comparisons were done in ohmic L-mode [20] and inter-ELM H-mode [21]. In the L-mode experiments, the comparison was done with low density and high $\bar{n}_e$ plasma. Inside the SOL midplane of high and low $\bar{n}_e$ plasma, T_i was of the order of a few tens eV and T_i/T_e was ~2. On the other hand, in the divertor region, T_i/T_e decreased from ~1.5 to ~1 with increase in $\bar{n}_e$. In low density plasma of $\bar{n}_e = 1.2\times10^{19}$ m^{-3}, T_i and T_e were around 15 eV and 10 eV, respectively. In relatively higher density plasma of $\bar{n}_e = 1.6\times10^{19}$ m^{-3}, T_i and T_e were around 5 eV. In the inter-ELM H-mode experiments, several types of discharges were conducted to compare the ratio of T_i/T_e in the divertor region. In double-null discharge, T_i/T_e at 5 cm from the LCFS decreased from 3 to 2 with increase in upstream collisionality $\nu^*_{SOL,LCFS}$ ~12.2 to ~15.3. The values of T_i were ~18 eV and ~10 eV with $\nu^*_{SOL,LCFS}$ ~12.2 and ~15.3, respectively.

As introduced above, experimental data of divertor T_i is a little even in the attached condition but according to the SOL T_i measurements, it is expected that divertor T_i with the low neutral density (i.e. attached condition) in the large tokamaks is higher than or equal to T_e and so will be in the future fusion reactors. In this context, it can be considered that T_i plays an important role in the physical mechanism of plasma detachment in the fusion devices. A decrease in T_i is important not only for the reduction of ion heat and particle flux on the divertor but also for a decrease in T_e. When the plasma density is high like that of divertor plasma, T_i and T_e are directly connected through energy relaxation process. In a linear divertor plasma simulator NAGDIS-II where T_i is much lower than T_e, it is suggested that one of key factors to decrease T_e is an energy transfer from

electrons to ions through the relaxation process [22]. If T_i is not so much lower than T_e, it is considered that T_e will not be decreased through the relaxation process. Therefore, it is important to decrease T_i for the reduction of T_e. Also, high T_i makes the temperature of neutral particles higher through charge-exchange or elastic collision process and then it can be expected that the higher temperature neutral particles make it more difficult to decrease temperature of charged particles. Although T_i can be considered to affect significantly on characteristics of plasma detachment, no direct measurement data of T_i exists. In order to clarify role of the high T_i on plasma detachment, detailed measurements of T_i such as spatial distribution and time evolution during detachment are important. Therefore, a simple T_i measuring method which enables multi-point measurement of the detached plasma is necessary.

1.4 Neutral particles in plasma detachment

In this section, importance of parameters of neutral particles including atoms and molecules in plasma detachment is focused on. Plasma detachment is achieved by the complex effect of atomic and molecular processes.

First, roles of neutral parameters in individual processes are introduced. As mentioned in Sec. 1.3, neutral energy affects ion energy through the charge-exchange or the ion-neutral elastic collision. The excited state of neutral atom affects the rate coefficients of the excitation and ionization as shown in atomic and molecular database of hydrogen species [23,24]. As for the molecular effect, the vibrational state of neutral hydrogen molecule (H_2) affects the rate coefficients of vibrational excitation, dissociation and ionization. These neutral parameters affect the loss energy of electrons through these processes. The volumetric recombination processes are roughly divided into two types: electron-ion recombination (EIR) and molecular activated recombination (MAR). EIR consists of three-body recombination (H^++e+e→H+e) and radiative recombination (H^++e→H+$h\nu$). MAR is volumetric recombination process associated with vibrationally excited molecule [25-28]. The MAR processes in hydrogen plasma are listed in Table 1.

Table 1. Reaction processes in molecular activated recombination (MAR).

• DA-MAR	·DA	$H_2(v) + e \rightarrow H^- + H$
	·MN	$H^- + H^+ \rightarrow H + H^*(n = 2,3)$
• IC-MAR	·IC	$H_2(v) + H^+ \rightarrow H_2^+(v) + H$
	·DR2	$H_2^+(v) + e \rightarrow H + H^*$
• MIC-MAR	·IC	$H_2(v) + H^+ \rightarrow H_2^+(v) + H$
	·MIC	$H_2(v) + H_2^+(v) \rightarrow H_3^+(v) + H$
	·DR3	$H_3^+(v) + e \rightarrow 3H,\ H_2(v) + H^*$

The DA-MAR consists of dissociative attachment (DA) and mutual neutralization (MN) process. The IC-MAR consists of ion conversion process of H_2 and H^+ (IC) and dissociative recombination of H_2^+ and electron (DR2). The MIC-MAR consists of IC process, another ion conversion process of H_2 and H_2^+ (MIC), and dissociative recombination of H_3^+ and electron (DR3). As it can be seen in cross section of each process [24-25], rate coefficients of the MAR depend on vibrational and rotational state of H_2. For example, rate coefficients of IC and DA reactions are introduced here.

Figure 1.4.1 shows IC rate coefficient with each vibrational level (v) of H_2. It should be also noted that the rate coefficient depends on T_i. The coefficients are calculated from cross section in Ref. [25]. The order of the coefficient is affected by v and T_i. In the T_i, range, the rate coefficient with lower v decreases with T_i by about an order. With higher v, the change of the coefficient with T_i is some factor. Figure 1.4.2 shows dependence of DA rate coefficient on T_e and rotational level (J) of H_2. The data of Ref. [29] are used. With increase in J, the rate coefficient increases by some orders.

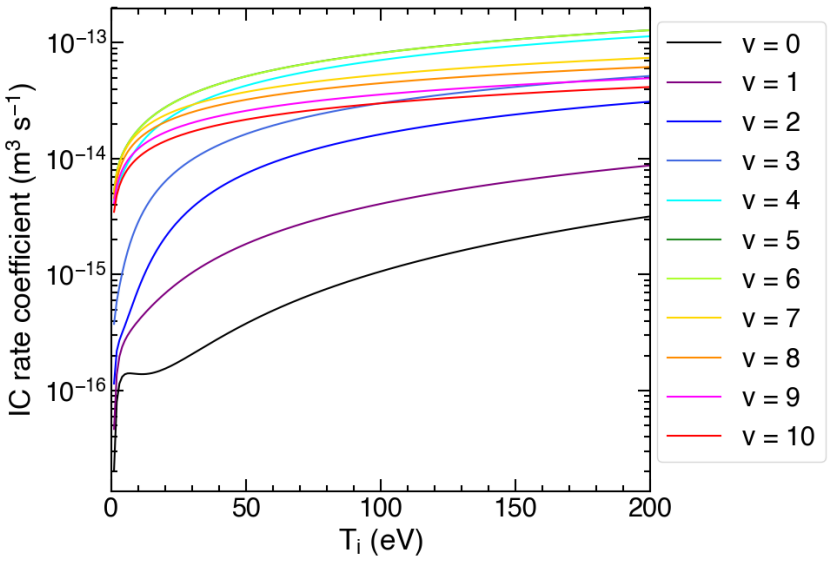

Figure 1.4.1. T_i dependence of rate coefficients of the IC reaction with some value of vibrational level (v) of H_2. The data are calculated by using cross section in Ref. [25].

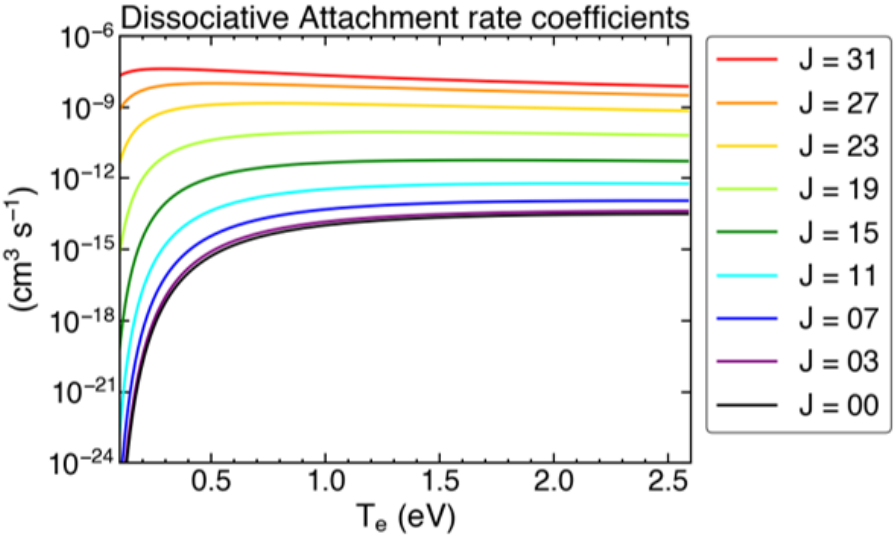

Figure 1.4.2. T_e dependence of rate coefficients of the DA reaction with some value of rotational level (J) of H_2. The data are taken from Ref. [29]

Next, experimental results of neutral parameters in plasma detachment are introduced. In Alcator C-Mod tokamak, effect of density and energy of neutral atom on plasma detachment was investigated [30]. Assuming that the detachment process was predicated on ion-neutral collisions removing ion momentum, neutral atom density was evaluated from plasma pressure gradient and the evaluated density was compared with neutral atom density obtained from spectroscopic measurement. It is suggested that atoms had high energy and that higher density was needed for the higher energy atoms to lead to detachment than the density of stationary atoms. This means the efficiency of the momentum removal in the case of strong coupling between ions and neutrals is lower than that in the case of weak coupling. As for the volumetric recombination, effectiveness of EIR in plasma detachment has been confirmed in all major tokamaks. Characteristic spectra of neutral atoms due to three-body recombination process were observed in tokamaks such as JET [31], JT-60U [32], ASDEX Upgrade [33] and Alcator C-Mod [34]. On the other hand, the contribution of MAR to plasma detachment in tokamak is not collectively understood both experimentally and numerically. In Alcator C-Mod, plasma sink due to MAR in plasma detachment is indicated to be comparable with that caused by EIR [34] and similar conclusions were also made in JT-60 U [35]. On the other hand, in ASDEX Upgrade, the contribution of MAR to the overall recombination rate is indicated to be of the order of 10 % [36].

As mentioned before, plasma detachment is achieved by the complex effect of atomic and molecular processes and thus it is rather difficult to investigate the effect of neutral parameters on plasma detachment. So far, many works including experiments and numerical simulations have contributed to the understanding of the effects of neutral pressure or density on plasma detachment. However, the experimental database on the effect of neutral parameters including the rovibrational states of H_2 and the temperature in addition to the density on the detachment is not sufficient. Therefore, it needs experiments to vary neutral states actively in addition to the neutral density and to investigate the effects of these neutral parameters as well as T_e and T_i on plasma detachment.

1.5Thesis objectives and outline

To understand physical mechanism of plasma detachment, T_i and neutral parameters including temperature, density and quantum states of atoms and molecules are important parameters. Since T_i of the SOL/Divertor plasma in the fusion devices can be high enough, T_i plays an important role in plasma detachment. However, T_i is not measured during the detached condition in existing tokamaks and detailed measurements of T_i such as spatial distribution and time evolution during detachment are important. Also, parameters of charged particles during detached condition are tightly connected to the neutral parameters. However, the experimental database on the effect of neutral parameters affected by charged particles on plasma detachment is not sufficient. Therefore, this study aims 1) to develop a simple T_i measuring method and 2) to clarify the neutral particle effect on plasma detachment.

For the aim 1), the object of this thesis is to develop a new T_i measuring method using a Langmuir probe. In general, LPs are used to measure basic plasma parameters such as T_e, n_e, and ion saturation current (I_{is}). This study focuses on the contribution of ion temperature parallel to the magnetic field ($T_{i\|}$) to I_{is}. Since I_{is} can be expressed as $0.5eSn\{(kT_e+\gamma kT_{i\|})/m_i\}^{1/2}$, where e is elementary charge, S is the effective area of the LP, n is the plasma density, γ is ion polytropic index, m_i is ion mass, there is a possibility to evaluate $T_{i\|}$ by using a LP when is $T_{i\|}$ high enough. Also, LPs have an advantage of simple structure and they are installed on divertor plates of most tokamaks. RFAs and ISPs are usually used to directly measure T_i of the SOL/Divertor plasma in the attached divertor condition. RFAs need its mesh size as small as Debye length. When the plasma is low temperature and high density like the detached divertor plasma, the Debye length becomes very short and it is difficult to use such a small mesh for RFAs. Also, when the neutral density is high, penetration of the gas into the RFA may happen. If the neutral density between the RFA grids is high, there are risks of plasma-gas interaction and of discharge in the RFA. ISPs tend not to reflect the correct T_i due to space charge limited condition when the plasma density is high. The LP as a $T_{i\|}$ diagnostic will be helpful tool for detailed measurements of detached plasma if the evaluation method is established.

For the aim 2), the object of this study is to change neutral parameters experimentally and to investigate its effect on plasma detachment by using neutral gas puff and pump. The neutral states depend on the amount of gas supply and pump since the balance between gas puff and pump affects replacement of room-temperature gas and neutral particles of which state is changed by plasma. Therefore, neutral states are expected to change by changing the balance between gas puff and pump. Figure 1.5.1 shows a conceptual drawing of the effect of gas puff and pump on neutral temperature. Here, water means the gas, fire means the plasma and leakage means the particle exhaust. Supplying water a lot with large leakage makes temperature of the water in the pot and

fire lower. This means that supplying gas a lot with strong pump makes temperature of neutral particles and plasma lower.

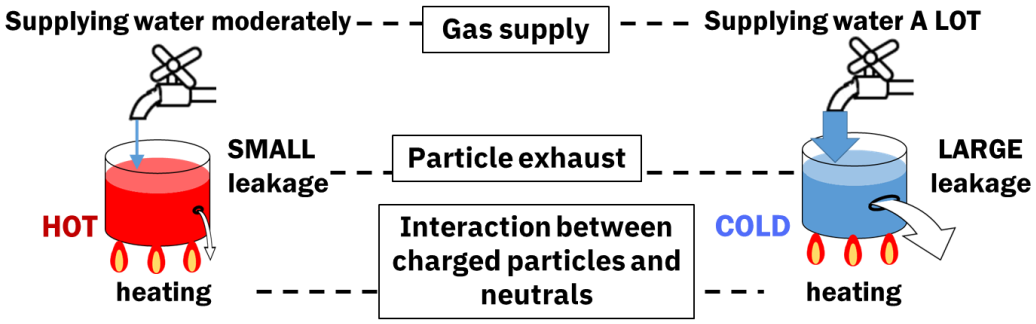

Figure 1.5.1 Conceptual drawing of the effect of gas puff and pump on neutral temperature.

To do the above fundamental researches on development of T_i evaluation method using a LP and on neutral effect of plasma detachment, the tokamak is not the best device to conduct experiments. For the fundamental research on detached plasma, linear divertor plasma simulators have contributed [37]. The plasma parameter regime of general linear devices is shown in Figure 1.5.2 based on Ref. [38]. The linear devices can produce low temperature and high density plasma and aims to simulate the detached divertor plasma. They can produce the plasma with open magnetic field configuration stationary. Compared with tokamaks, the linear devices can specialize in fundamental research on edge plasma physics and flexible measurements with high controllability can be done. So far, linear devices have contributed to the understanding of edge plasma physics such as demonstration of plasma detachment by gas injection and detail measurements of atomic and molecular processes in the detached plasma. However, the general linear devices cannot investigate the physics in the high temperature regime since they cannot produce high temperature plasma due to absence of plasma confinement region or of high power heating system. Moreover, in the low temperature regime, while T_i in the tokamaks is expected to be higher than or equal to T_e, T_i of the general linear devices is much lower than T_e. In order to solve the subject I and II, fundamental research using a device which has high temperature plasma like the SOL/Divertor plasma and which enables flexible measurements with high controllability like the general linear devices is needed.

In GAMMA 10/PDX tandem mirror of University of Tsukuba, divertor simulation experiments have been carried out by using an end-loss plasma which has higher $T_{i\parallel}$ than T_e [39-41]. The plasma parameter regime of GAMMA 10/PDX without additional gas injection is also shown in Figure 1.5.2. The $T_{i\parallel}$ range can be widely changed by using confinement region, heating

system and gas puff system. It is expected that the plasma is suitable for developing the measuring method of $T_{i\parallel}$ by using a Langmuir probe experimentally. Also, plasma detachment associated with MAR has been confirmed and spatial characteristics of the detached plasma have been studied [41-43]. The scale length toward the target plate in GAMMA 10/PDX is longer than other linear devices and there are strong pumping systems including cryopumps [44]. Thus, it can keep the source plasma rather stable and it considered to be able to change neutral parameters in the downstream by gas puff and pump.

This thesis consists of 4 Chapters. After this Chapter 1, experimental setup such as GAMMA 10/PDX and $T_{i\parallel}$ evaluation principle by using a Langmuir probe is described in Chapter 2. Results of studies on development of T_i measurement using a Langmuir probe and on neutral particle effect on plasma detachment using gas puff and pump are described in Chapter 3. Finally, conclusion is presented in Chapter 4.

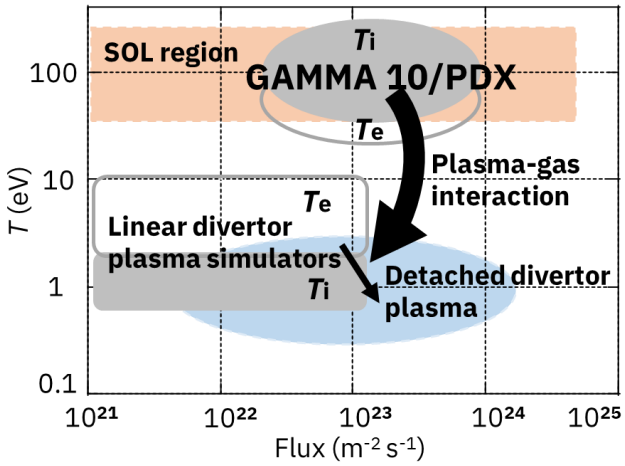

Figure 1.5.2 Plasma parameter regime of general linear divertor plasma simulators and of GAMMA 10/PDX compared with SOL region of torus device. (based on Ref. [38].)

Chapter 2

Experimental device and diagnostics

2.1 GAMMA 10/PDX tandem mirror

A brief introduction of the experimental device GAMMA 10/PDX tandem mirror is written in this section. Details of GAMMA 10/PDX is written in Refs. [38-41].

2.1.1 Vacuum vessel, magnetic field distribution and pumping system

A schematic view of GAMMA 10/PDX is shown in Figure 2.1.1 (a). GAMMA 10/PDX is a tandem mirror device, which is composed of a central cell, anchor cells, barrier cells, plug cells and end regions. The entire length of the device is 27 m and the total volume of the vacuum vessel is 150 m^3.

Figure 2.1.1 (b) shows the magnetic field distribution of GAMMA 10/PDX. Main confinement mirror magnetic field is formed in the central cell. Near the midplane of the central cell, the uniform magnetic field is formed by ten solenoid coils and stronger magnetic field is generated at the ends of the cell. In the anchor cells, minimum-B configuration is formed by baseball coils to keep the plasma magnetohydrodynamically stable. In the plug/barrier cells, mirror configuration is adopted. In the case of experiments to improve plasma confinement in the central cell, electron cyclotron resonance heating (ECRH) and/or neutral beam injection (NBI) are applied in the plug/barrier cells to change the plasma potential distribution in axial direction, which is not applied in experiments of this thesis. In the east and west end region, the magnetic field is diverging toward each end where solid metal plates are mounted to terminate the plasma.

Main pumping system used in recent experiments of GAMMA 10/PDX is composed of turbo-molecular pumps (TMPs) and helium cryosorption pump systems (CPs). A total of six TMPs are

installed. One TMP is mounted in each anchor cell and end region and two TMPs are mounted in the central cell. The TMPs in the two end region and one of TMPs in the central cell have the pumping speed of 1500 L/s and the other three TMPs have the pumping speed of 2500 L/s.
Base pressures without the plasma in the central cell, anchor cells, plug/barrier cells and the two end region are in the range of 1×10^{-5} Pa, 1×10^{-5} Pa, 6×10^{-6} Pa and 7×10^{-6} Pa, respectively.

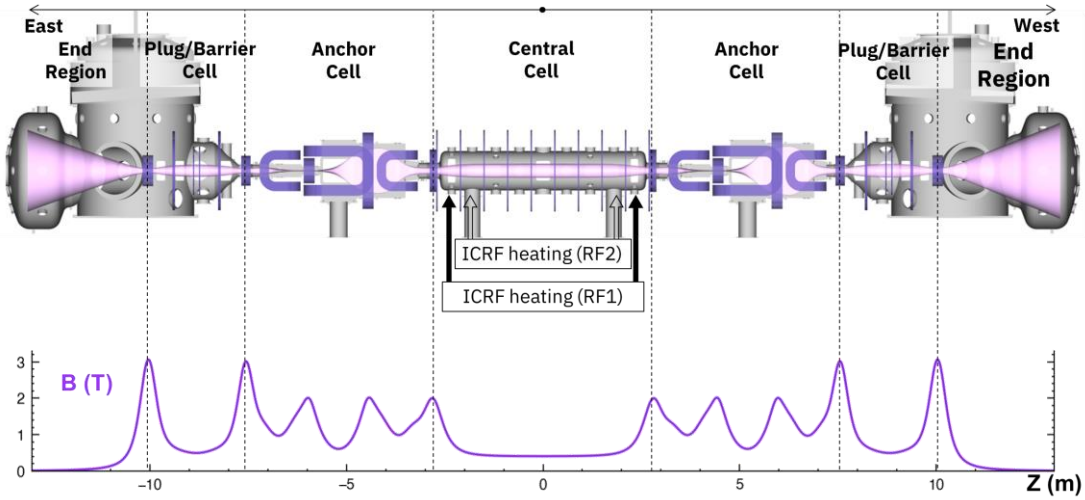

Figure 2.1.1 Schematic view of (a) GAMMA 10/PDX and (b) its magnetic field distribution

2.1.2 Plasma production and heating system

The initial plasma is injected toward the central cell in axial direction by magneto plasma dynamic (MPD) arc jet type plasma guns which are installed in the end region. In recent experiments, the one installed in the west end region is used. The plasma is sustained by applying ion cyclotron range of frequency (ICRF) wave heating with hydrogen gas puff.

In a standard operation, two types of ICRF heating systems installed in the central cell are used. One is called RF1 and the other is called RF2. The RF1 is used to generate the plasma and to heat the plasma in the anchor cells by ICRF fast waves with frequency of around 10 MHz. The RF2 is used to heat the plasma in the central cell by ICRF slow waves with frequency of ~6.36 MHz which is the ion cyclotron resonance frequency near the midplane of the central cell.

Main gas puff systems to product and sustain the plasma are installed in the central cell. The hydrogen gas is injected through the gas box surrounding the plasma. Timing and duration of the gas puff are controlled by piezoelectric valve.

In typical discharges, the plasma is sustained for 200 or 400 ms.

2.1.3 Divertor simulation experimental module (D-module)

In order to study plasma boundary physics such as plasma detachment, divertor simulation experimental module (D-module) is installed in the west end region of GAMMA 10/PDX. Figure 2.1.2 shows the schematic view inside of the D-module. The D-module consists of stainless-steel cuboid chamber with an inlet hole and a V-shaped target. The size of the cuboid is 480 mm × 500 mm × 700 mm for X, Y and Z directions. The size of each side of the V-shaped target is 300 mm × 350 mm and the tungsten plates with the thickness of 0.2 mm are attached on the exposure surface of the target base. The open angle of the V-shaped target can be adjusted and it is fixed to 45 degrees in the experiment of the thesis. Gas supply pipes are installed near the inlet of the D-module and are connected to a gas reserver tank via a piezoelectric valve. The amount of gas supply can be controlled by adjusting the pressure in the tank (plenum pressure). Timing and duration of the gas supply can be controlled by adjusting the opening of the piezoelectric valve. At the back side of the D-module, an exhaust orifice with a door covering the hole (exhaust door) is installed. When the exhaust door is open, neutral gas is drained to the outside of the D-module through the orifice and then pumped at the cryosorption pumps and turbo molecular pumps in the end region.

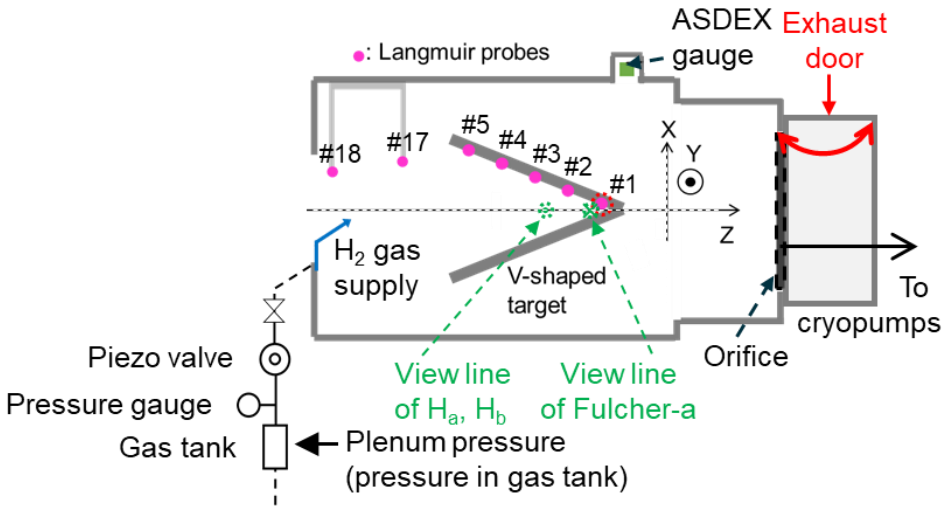

Figure 2.1.2. Schematic view of divertor simulation experimental module (D-module). In this figure, side wall of the D-module is not drawn.

As shown in Figure 2.1.3, the vertical position of the D-module in the west end region can be moved by elevating system. When the D-module is far below the horizontal axis of GAMMA 10/PDX, the plasma is terminated at the end plates. When the D-module is on the axis, the plasma is terminated at the V-shaped target.

On the roof of the D-module, another target plate called roof target is also installed as shown in Figure 2.1.4.

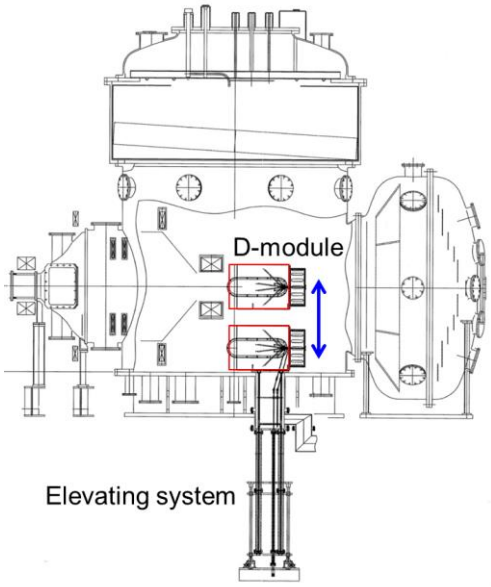

Figure 2.1.3. Schematic view of the west end region, D-module and its elevating system.

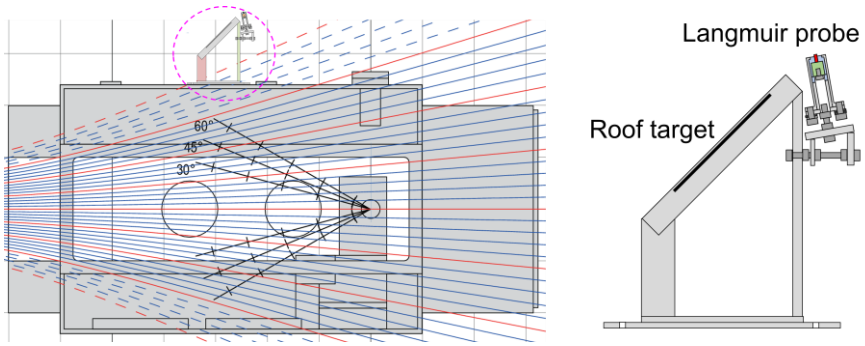

Figure 2.1.4. Schematic view of the D-module and the roof target.

2.2 Diagnostics

In this section, diagnostics used in this thesis are introduced. First, overview of each diagnostic is written. Then, details of important diagnostics in this thesis are introduced.

2.2.1 Diagnostics overview

Fundamental diagnostics of the plasma in the central cell are the diamagnetic loop and the microwave interferometer. The diamagnetic loop is a diagnostic to measure diamagnetism representing pressure of the central cell plasma by using the diamagnetic property of the plasma. The microwave interferometer is a diagnostic to measure electron line density by using the density dependence of phase of microwave propagating inside the plasma. The microwave interferometers are also installed in the anchor cells, plug/barrier cells and the west end region. Near the end plates in the east and west end region, End Loss Ion Energy Analyzers (ELIEAs) are installed to measure distribution of ion energy parallel to the magnetic field. Near the end plates in the east end region, End Loss Energy Components Analyzer (ELECA) is installed to measure velocity distributions parallel and perpendicular to the magnetic field.

In the D-module, thirteen Langmuir probes (LPs) are installed on the upper side of the V-shaped target as shown in Figure 2.2.1 and two LPs are installed near the inlet as shown in Figure 2.1.2. The detail of LP method is introduced in subsection 2.2.2. Two kinds of spectroscopic measurement systems are installed in the D-module. One has a view line near the center of the D-module and it uses a spectrometer USB 2000+ of Ocean Optics, Inc. The other has ten channel view lines and it uses a spectrometer Shamrock500i of ANDOR Co., Ltd. The view lines of each spectroscopic system are shown in Figure 2.2.2. Shamrock500i has better wavelength resolution than USB2000+ and it enables to identify lines of Fulcher-α band spectra of hydrogen molecules. On the top side in the D-module, ASDEX type fast ionization gauge is installed to measure neutral pressure in the magnetic field. Near the roof target mounted on the D-module, an LP is also installed as shown in Figure 2.1.4.

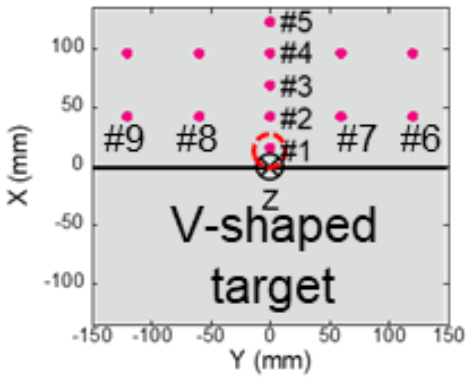

Figure 2.2.1 Schematic of Langmuir probe array on the upper side of the V-shaped target in the D-module.

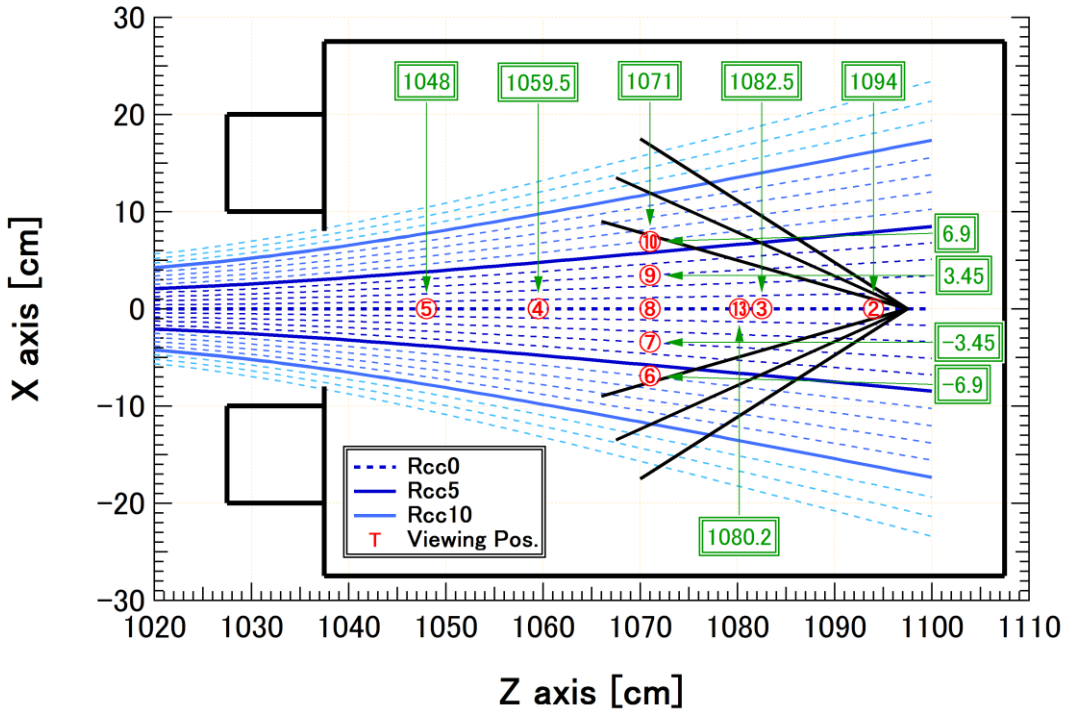

Figure 2.2.2 View lines of spectroscopic measurement system in the D-module.

2.2.2 Langmuir probe

In this subsection, basic principle of Langmuir probe (LP) method and method to evaluate the product of ion temperature parallel to the magnetic field and ion polytropic index is introduced. The latter method is one of research subjects of this thesis. Here, following equations represent that of hydrogen plasma.

2.2.2.1 Basic principle

By varying voltage bias applied to an LP, a probe current (I_p)-voltage (V_p) characteristic as shown in Figure 2.2.3 is obtained. In the range of sufficiently negative V_p, electrons are reflected before reaching the LP and I_p becomes ion saturation current (I_{is}). To satisfy the Bohm criterion, ion flow speed entering the LP becomes ion sound speed (C_s) and I_{is} can be written as

$$I_{is} = \frac{1}{2} S e n_e \sqrt{\frac{kT_e + \gamma k T_{i\parallel}}{m_i}}. \quad (2.1)$$

Here, S, e, n_e, k, T_e, $T_{i\parallel}$, γ and m_i are the effective probe surface area, elementary charge, electron density, Boltzmann constant, electron temperature, ion temperature parallel to the magnetic field and ion polytropic index, respectively. The coefficient 1/2 of Eq. (3.1) is the ratio of density at the sheath edge to that in the upstream derived from the conservative form of the momentum equation [45]. In the range of sufficiently positive V_p meaning V_p is higher than or equal to plasma potential (V_s), all electrons are collected and I_p becomes sum of I_{is} and electron saturation current (I_{es}), that is,

$$I_p = I_{es} - I_{is}. \quad (2.2)$$

The I_{es} can be written as

$$I_{es} = \frac{1}{4} S e n_e \sqrt{\frac{8kT_e}{\pi m_e}}. \quad (2.3)$$

Here, S of I_{is} and that of I_{es} are assumed to be the same. In the range of V_p lower than electron saturation range and higher than ion saturation range, I_p becomes sum of I_{is} and electron current (I_e) of which value changes with V_p.

$$I_p = I_e - I_{is} \quad (2.4)$$

and

$$I_e = I_{es} \exp\left[\frac{eV_p}{kT_e}\right] = \frac{1}{4} S e n_e \sqrt{\frac{8kT_e}{\pi m_e}} \exp\left[\frac{eV_p}{kT_e}\right]. \quad (2.5)$$

When $I_e = I_{is}$, I_p becomes zero and V_p in this situation is called floating potential (V_f).

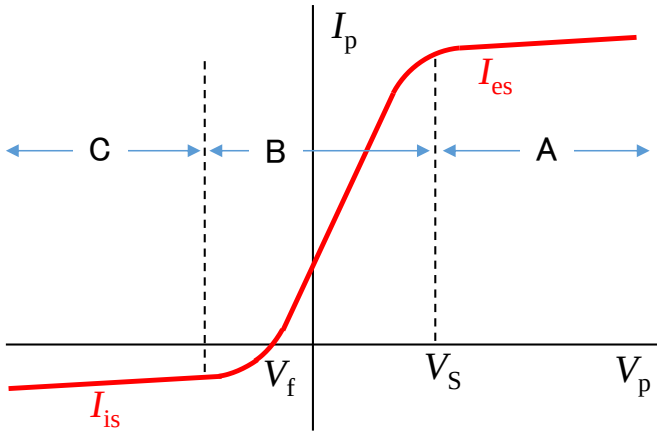

Figure 2.2.3 Schematic of a current-voltage characteristic of Langmuir probe.

As for determination of T_e, n_e and V_s, V_p dependence of I_{is} is first fitted to a linear line. Then, T_e is first obtained from a I_e-V_p characteristic by using the linear fitted I_{is} and equations (2.4) and (2.5). The V_s is obtained from the cross point of fitting lines of I_e and I_{es}. Then, the value of I_e at $V_p = V_s$, is I_{es} and n_e is obtained by using the values of I_{es}, T_e and equation (2.3)

2.2.2.2 Evaluation of the product of ion temperature parallel to the magnetic field and ion polytropic index

In this study, $\gamma T_{i\parallel}$ is evaluated by following equation obtained by combining equations (2.1) and (2.3).

$$\gamma T_{i\parallel} = \left[\frac{2m_i}{\pi m_e}\left(\frac{I_{is}}{I_{es}}\right)^2 - 1\right] T_e \qquad (3.6)$$

The value of I_{is} is derived from the value of linear fitted current at $V_p = V_f$ to avoid the error resulting from sheath expansion.

Chapter 3

Results and discussion

In this chapter, experimental results obtained in GAMMA 10/PDX and discussion are described. Results and discussion of Development of T_i evaluation method using a Langmuir probe is described in section 3.1. In section 3.2, results and discussion of investigation of neutral particle effect on plasma detachment using gas puff and pump are described.

3.1 Development of T_i evaluation method using a Langmuir probe

In this section, characteristic of $\gamma T_{i\|}$ evaluated by using a Langmuir probe (LP) when $T_{i\|}$ is varied is experimentally investigated in order to develop the measuring method of $T_{i\|}$ by using an LP. A comparison between $\gamma T_{i\|}$ evaluated by using an LP and $T_{i\|}$ measured by an ion energy analyzer (ELIEA).

3.1.1 T_i variation by ICRF heating and additional gas puff in the central cell

In this experiment, $T_{i\|}$ of the plasma in the west end region was varied by ICRF heating which heats the plasma in the central cell (RF2) and the additional hydrogen gas puff in the central cell. Here, two types of plasma discharges were conducted. In the both discharges, another ICRF heating which produces the plasma in the central cell and heats the plasma in the anchor cells (RF1) was applied. One of the discharges was conducted with RF2 and the other was without RF2. The plasmas were produced and sustained for 200 ms from time t = 50 ms. The additional hydrogen gas in the central cell was supplied from t = 160 to 240 ms at the plenum pressure of 70 Torr.

Figure 3.1.1 shows time evolution of (a) diamagnetism and (b) electron line density of the central cell plasma (DM_{CC} and NL_{CC}, respectively), (c) $T_{i\parallel}$ and (d) particle flux parallel to the magnetic field near the end plate measured by ELIEA ($T_{i\parallel,IEA}$ and $\Gamma_{i\parallel,IEA}$, respectively). Typical time evolution of DM_{CC} and NL_{CC} during each one discharge are shown in Fig. 3.1.1. From t = 220 ms, electron cyclotron resonance heating is applied in the central cell but it is outside the scope of this thesis. Data of $T_{i\parallel,IEA}$ and $\Gamma_{i\parallel,IEA}$ are averaged value over almost the same three discharges.

To investigate the effect of RF2, plasmas with and without RF2 during the period from t = 100 ms to t = 160 ms are compared. In the discharge with RF2, DM_{CC} and NL_{CC} are higher than those without RF2, indicating that T_i of the plasma in the central cell is higher than that without RF2. In the west end region, both $T_{i\parallel,IEA}$ and $\Gamma_{i\parallel,IEA}$ with RF2 are higher than those without RF2. With RF2, a high ion temperature component was identified in the energy spectra measured by ELIEA and it was not identified without RF2. The details of the temperature component are described in subsection 3.1.3. In the period, $T_{i\parallel,IEA}$ with and without RF2 are ~240 eV and ~140 eV, respectively. The values of $T_{i\parallel,IEA}$ with RF2 are the effective value which is evaluated from the convolution of the high and low ion temperature components.

Next, to investigate the effect of the additional gas puff in the central cell, the plasma with RF2 during the period from t = 100 ms to t = 160 ms and that during the period from t = 185 ms to t = 220 ms are compared. When the additional gas is supplied, DM_{CC} decreases and NL_{CC} increases. In the end region, $T_{i\parallel,IEA}$ and $\Gamma_{i\parallel,IEA}$ decreases. When the gas is supplied, $T_{i\parallel,IEA}$ decrease to ~130 eV.

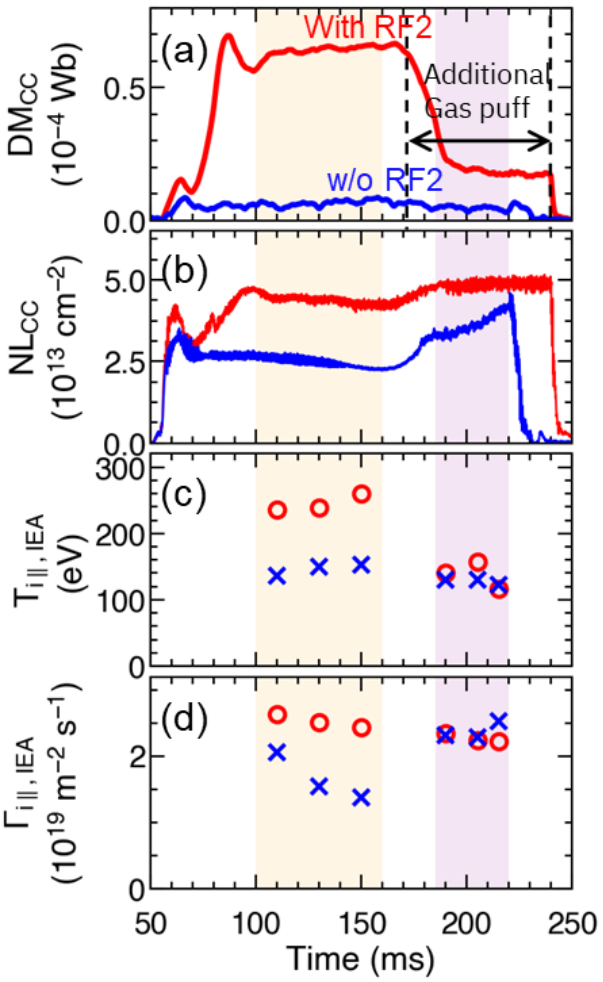

Figure 3.1.1 Time evolution of (a) diamagnetism and (b) electron line density of the central plasma, (c) ion temperature parallel to the magnetic field and (d) ion particle flux near the end plate measured by ELIEA in the west end region. Red lines and circles: the discharge with RF2 and blue lines and crosses: the discharge without RF2.

3.1.2 Langmuir probe analysis of $\gamma T_{i\|}$

In the end region, Langmuir probe measurements were also conducted by using an LP installed near the roof target on the D-module. Figure 3.1.2 shows a typical LP current-voltage (I_p-V_p) characteristic measured at t = 120-140 ms in the same discharge as those of ELIEA data with RF2. The I_p-V_p characteristic contains clear ion saturation current (I_{is}) region and electron saturation current (I_{es}) region.

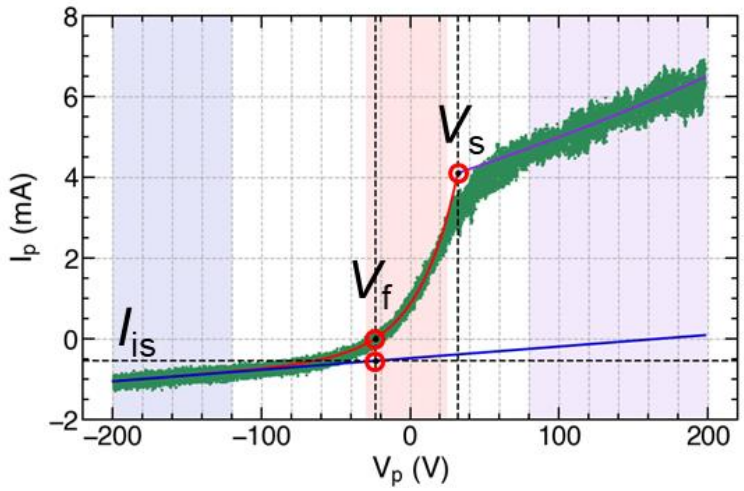

Figure 3.1.2 A typical current-voltage characteristics of the Langmuir probe.

From the I_p-V_p characteristic, each parameter was evaluated. Figure 3.1.3 shows time evolution of (a) T_e, (b) n_e, (c) I_{is}, (d) I_{es} and (e) $(I_{is}/ I_{es})^2$. Each data was measured in the same discharge as those of ELIEA. Each error bars are taken from the fitting error of the characteristics.

Again, plasmas with and without RF2 during the period from t = 100 ms to t = 160 ms are compared to investigate the effect of RF2. In the period, T_e and n_e with RF2 is higher than that without RF2. In order to evaluate $\gamma T_{i\|}$ by using Eq. (2.6), one of the important parameters is $(I_{is}/ I_{es})^2$. The value of $(I_{is}/ I_{es})^2$ with RF2 is lower than that without RF2 during the discharge. Substituting the above T_e and $(I_{is}/ I_{es})^2$ for Eq. (2.6), $\gamma T_{i\|}$ was evaluated. Figure 3.1.3 (f) shows time evolution of $\gamma T_{i\|}$ obtained from the LP ($\gamma T_{i\|,LP}$). During the period, $\gamma T_{i\|,LP}$ with RF2 is lower than that without RF2. The values of $\gamma T_{i\|,LP}$ with and without RF2 are ~440 eV and ~620 eV, respectively.

Next, the plasma with RF2 during the period from t = 100 ms to t = 160 ms and that during the period from t = 185 ms to t = 220 ms are compared to investigate the effect of the additional

gas puff. When the additional gas is supplied, T_e decreases and n_e with RF2 slightly decreases. At the same time, $\gamma T_{i\parallel,LP}$ decreases to ~300 eV.

In the downstream where ELIEA is installed, $T_{i\parallel}$ with RF2 is higher than that without RF2, however, near the roof target, $\gamma T_{i\parallel}$ with RF2 is lower than that without RF2. The difference in value of $\gamma T_{i\parallel,LP}$ between the discharges with and without RF2 can be considered to be caused by the difference in γ and/or $T_{i\parallel}$, which is discussed in the following subsection.

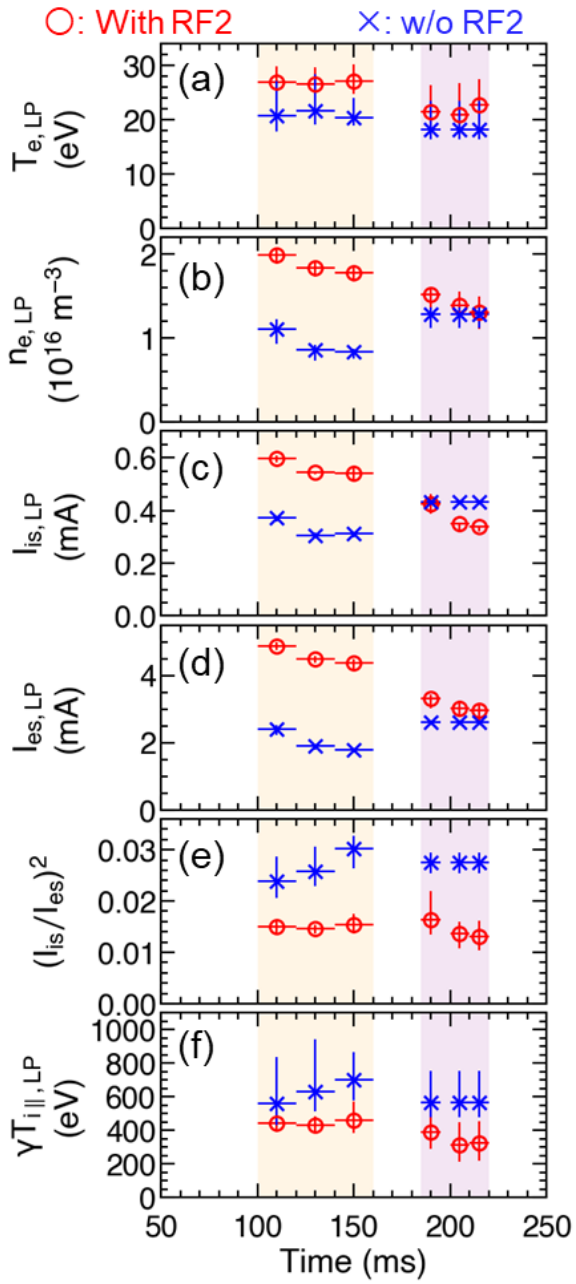

Figure 3.1.3 Time evolution of (a) electron temperature, (b) density, (c) ion saturation current, (d) electron saturation current, (e) the square of the ratio of ion saturation current to electron saturation current ($(I_{is}/ I_{es})^2$) and (f) the product of ion polytropic coefficient and temperature parallel to the magnetic field ($\gamma T_{i\parallel}$) evaluated by a Langmuir probe. Red circles: with RF2 and blue crosses: without RF2.

3.1.3 Evaluation of ion polytropic coefficient γ

In order to consider the reason for the difference in value of $\gamma T_{i\parallel,LP}$, the value of $T_{i\parallel}$ near the LP is discussed first. There is no diagnostic to measure $T_{i\parallel}$ near the LP and therefore the value is discussed here. In the end region, the magnetic field (B) is diverging. The magnitude of B near the LP is ~0.2 T and downstream B near ELIEA is ~0.01 T. Basic physics to determine the energy spatial distribution in the nonuniform magnetic field is conservation of magnetic moment and kinetic energy where the perpendicular energy is converted into or from the parallel energy. Therefore, ion temperature perpendicular to B ($T_{i\perp}$) is also important for considering ion temperatures parallel to B at the different B positions. In this study, $T_{i\perp}$ near the ELIEA is evaluated by using ELECA installed in the east end region. Though ELIEA used here is installed in the west end region, $T_{i\parallel}$ in the east and west position was almost the same. Upper limit of $T_{i\perp}$ with and without RF2 were ~0.76 eV and ~0.66 eV, respectively. The ratio of B at the LP to B at ELECA is about 0.2/0.01 = 20. Assuming that $T_{i\perp}$ in the east and west end is almost the same and that average perpendicular energy perpendicular to B is almost the same as $T_{i\perp}$, upper limit of $T_{i\perp}$ at the LP with and without RF2 becomes ~15 eV and ~13 eV, respectively and these become maximum differences in $T_{i\parallel}$ between the LP and ELIEA. Since these differences are smaller than the errorbar of $T_{i\parallel}$, differences in $T_{i\parallel}$ between the LP and ELIEA cannot be discussed here.

Next, the value of γ is evaluated by dividing $\gamma T_{i\parallel,LP}$ by $T_{i\parallel}$ measured by ELIEA. Figure 3.1.4 (a) shows time evolution of the evaluated γ. The evaluated γ with RF2 is lower than that without RF2. When the additional gas in the central cell is puffed, γ with RF2 increases. Since the values of $\gamma T_{i\parallel,LP}$ have large errors due to the fitting errors of I_p-V_p characteristics, here the qualitative tendency where γ with RF2 is lower than that without RF2 and γ with RF2 increases when the gas was supplied.

In the beginning, the characteristics of γ in the widely used plasma fluid model [45-47] is considered. In the model, the value of γ changes with the ion-ion collisionality $L/\lambda_{i\text{-}i} \propto n/T_i^2$. With increase in n/T_i^2, the value of γ decreases from 3 to 1. Figure 3.1.4 (b) shows time evolution of $n_e/T_{i\parallel}^2$. This value is calculated from n_e measured by the LP and $T_{i\parallel}$ measured by ELIEA. With and without RF2, $n_e/T_{i\parallel}^2$ is almost the same value and $n_e/T_{i\parallel}^2$ with RF2 increases when the gas is supplied. From the point of view of time scale, the ion-ion collision time was also evaluated by $\tau_{i\text{-}i} = \{3^{1/2}6\pi\varepsilon_0^2 m_i^{1/2}(kT_{i\parallel})^{3/2}\}/\{e^4 n_i \ln[\Lambda]\}$. Here, $\ln[\Lambda]$ is coulomb logarithm and the equation is in the case of hydrogen plasma ($Z = 1$). All of $\tau_{i\text{-}i}$ are greater than or equal to ~400 ms, which is longer than the discharge time (200 ms) and this means that the plasma in the both cases were always collisionless. Note that the effect of the collision between ions and the neutrals on γ in the end region is also considered to be negligible since the neutral density in the end region was low enough and the ion mean free path was much longer than the device length. Therefore, it seems

that the difference in value of γ between the discharges with and without RF2 is caused by other reason.

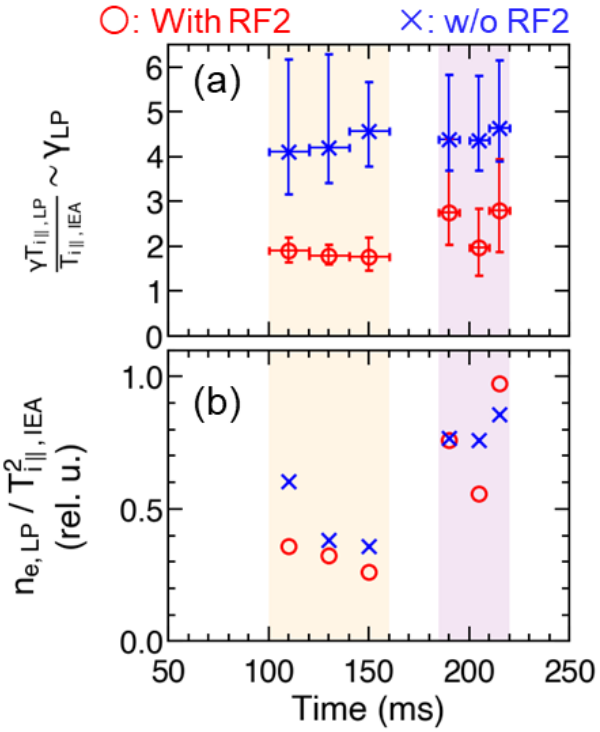

Figure 3.1.4 Time evolution of (a) evaluated ion polytropic coefficient and (b) $n_e/T_{i\parallel}^2$ which is proportional to collisionality.

Then, the effect of ion temperature on γ as mentioned in kinetic simulation results [48] is considered. In the work, it is suggested that a high ion temperature of collisionless plasma would make γ much lower than the value in the widely used plasma fluid model.

Figure 3.1.5 shows normalized energy spectra obtained by ELIEA (a) with RF2 and (b) without RF2. Each spectrum was measured from t = 120-140 ms with and without RF2 and normalized by each peak value. In the discharge without RF2, the energy spectrum is well fitted to single Maxwellian distribution of $T_{i\parallel}$ ~150 eV. On the other hand, the spectrum with RF2 can not be fitted to single Maxwellian and is well fitted to the convolution of two Maxwellian distributions of $T_{i\parallel}$ ~130 eV and ~570 eV. It indicates that ICRF heating in the central cell makes high temperature component in the ion energy distribution in the end region.

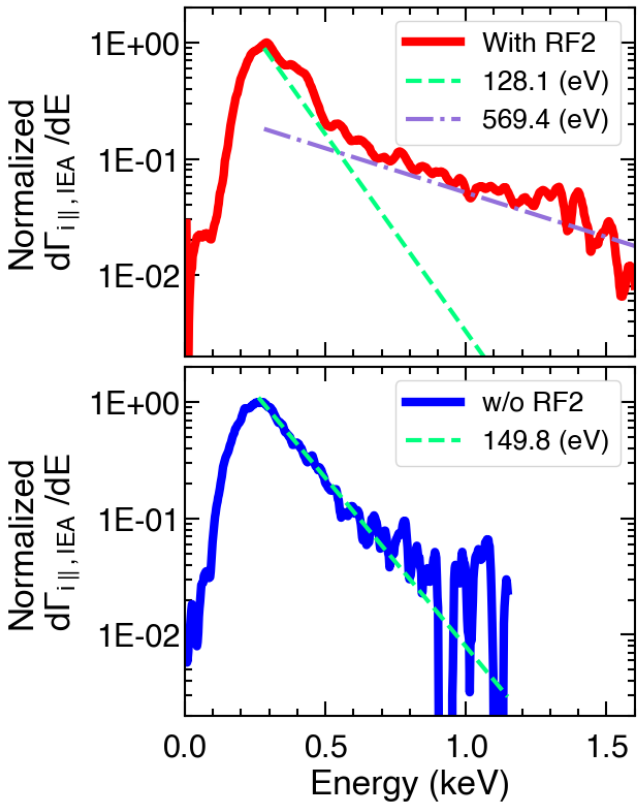

Figure 3.1.5 Normalized ion energy spectra (a) with RF2 and (b) without RF2 measured by ELIEA. Single Maxwellian distribution fitting or convolution of two Maxwellian distributions fitting lines are also plotted.

Next, Figure 3.1.6 shows normalized energy spectra obtained by ELIEA (a) with RF2 and (b) with RF2 during the gas puff period. The spectrum with RF2 is the same as Fig. 3.1.5 (a). The spectrum with the gas puff was measured from t = 210-220 ms and normalized by the peak value. When the additional gas was supplied in the central cell, the energy spectrum was rather noisy and the high temperature component could not be detected. Anyway, the gas puff makes $T_{i\|}$ in the end region lower.

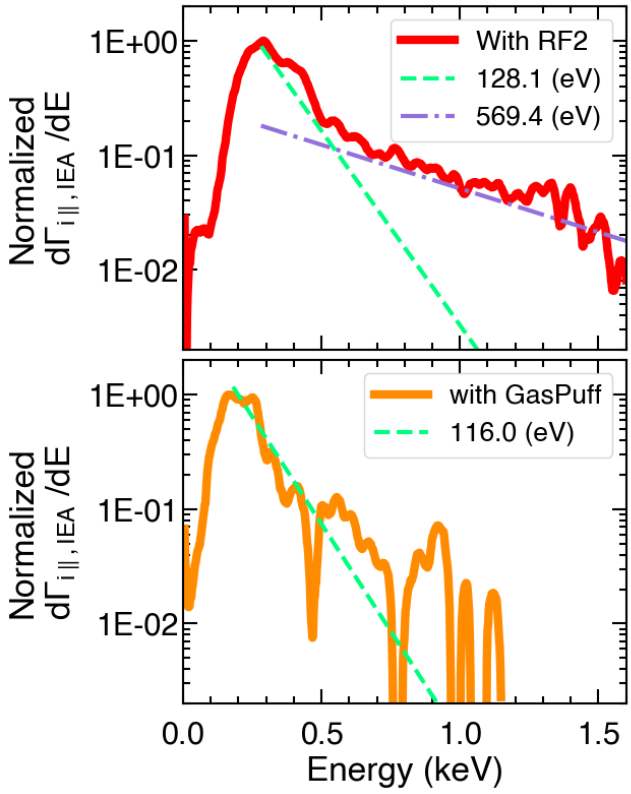

Figure 3.1.6 Normalized ion energy spectra (a) with RF2 and (b) without RF2 measured by ELIEA. Single Maxwellian distribution fitting or convolution of two Maxwellian distributions fitting lines are also plotted.

In this study, characteristic of $\gamma T_{i||}$ evaluated by using an LP when $T_{i||}$ was around 120 eV and around 250 eV with high temperature component was investigated. In light of the effects of RF2 and gas puff, it is experimentally suggested that γ changes with $T_{i||}$. Therefore, to improve quantitativity in evaluation of $T_{i||}$ using a Langmuir probe, expansion of database on the value and characteristics of γ by experiments and kinetic simulation is considered to be an effective method. This is a future work.

3.1.4 Summary

The objective of this study is to develop the measuring method of $T_{i\parallel}$ by using an LP. Characteristic of $\gamma T_{i\parallel}$ evaluated using an LP when $T_{i\parallel}$ is varied were experimentally investigated in GAMMA 10/PDX. Utilizing the high T_i plasma, an experiment to vary $T_{i\parallel}$ in the end region by using ICRF heating of the central plasma (RF2) and additional gas puff in the central cell was conducted. By using an LP, $\gamma T_{i\parallel}$ was evaluated and it was compared with $T_{i\parallel}$ measured by an ion energy analyzer. Applying ICRF heating in the central cell (RF2), $T_{i\parallel}$ measured by the analyzer ($T_{i\parallel,IEA}$) increased and $\gamma T_{i\parallel}$ evaluated by the LP ($\gamma T_{i\parallel,LP}$) decreased. When the additional gas was supplied in the central cell in addition to RF2, both $T_{i\parallel,IEA}$ and $\gamma T_{i\parallel,LP}$ decreased. The difference in tendency between $\gamma T_{i\parallel,LP}$ and $T_{i\parallel,IEA}$ was expected to be caused by the difference in γ and then the value of γ was evaluated by dividing $\gamma T_{i\parallel,LP}$ by $T_{i\parallel,IEA}$. While γ in general plasma-fluid model changes with collisionality, γ in this experiment changed even though collisionality did not changed. The results experimentally suggest that without changes in the ion-ion collisionality and ion-neutral collisionality, γ decreases with increase in $T_{i\parallel}$ due to a high ion temperature component. To improve quantitativity in evaluation of $T_{i\parallel}$ using a Langmuir probe, expansion of database on the value and characteristics of γ by experiments and kinetic simulation is considered to be an effective method. This is a future work.

3.2 Investigation of neutral particle effect on plasma detachment using gas puff and pump

In this section, effect of ion temperature and neutral states on plasma detachment associated with molecular activated recombination (MAR) are studied. Characteristics of plasma detachment depend not only on T_i and T_e but also on parameters of neutral atoms and molecules. These ion, electron and neutral parameters are tightly connected due to plasma-neutral interactions in plasma detachment. An experiment has been conducted to vary these parameters by combining H_2 gas puff and pump from the D-module through the exhaust door in the GAMMA 10/PDX as shown in Figure 2.1.2 in subsection 2.1.3.

3.2.1 Overview of the experiment

The experiment was conducted with the exhaust door closed and open, respectively. Additional H_2 gas was supplied to the plasma in the D-module when the exhaust door was closed and fully open. When the door was open, it was necessary to supply more H_2 gas to decrease T_e to almost the same value as that with the door closed. The H_2 gas was supplied at the plenum pressures of 750 and 1200 mbar with the door closed and open, respectively. Figure 3.2.1 shows typical time evolution of (a)diamagnetism of the plasma in the central cell (DM_{CC}), (b)electron line density of the plasma in the west plug region (NL_{WP}), (c)total gas pressure in the D-module (P_n), (d)T_e, (e)n_e and (f)I_{is}. The above T_e, n_e and I_{is} were measured by the probe #1 near the corner of the V-shaped target in the D-module as shown in Figure 3.1.2. Plasmas are produced and sustained for 400 ms by ICRF heating. The piezoelectric valve is opened from 10 ms after the beginning of plasma discharge to the end of it. During the discharges, DM_{CC} does not change so much and NL_{WP} increases with time due to the escaping gas from the D-module. After time (t) ~400 ms, The values of DM_{CC} and NL_{WP} with the door open are almost the same as those with the door closed, indicating that upstream plasma of the D-module are almost the same. Near the corner of the V-shaped target in the D-module, both T_e monotonically decreases from ~20 eV to ~2 eV. At the same position, n_e and I_{is} first increases and then decreases, which is called rollover, indicating that the plasma is being detached. When the door is open, the decrement of n_e and I_{is} after the rollover is smaller than that with the door closed. The upstream plasma is almost the same in the both cases but there is a difference in the degree of plasma detachment near the corner of the V-shaped target between the cases with the door open and closed.

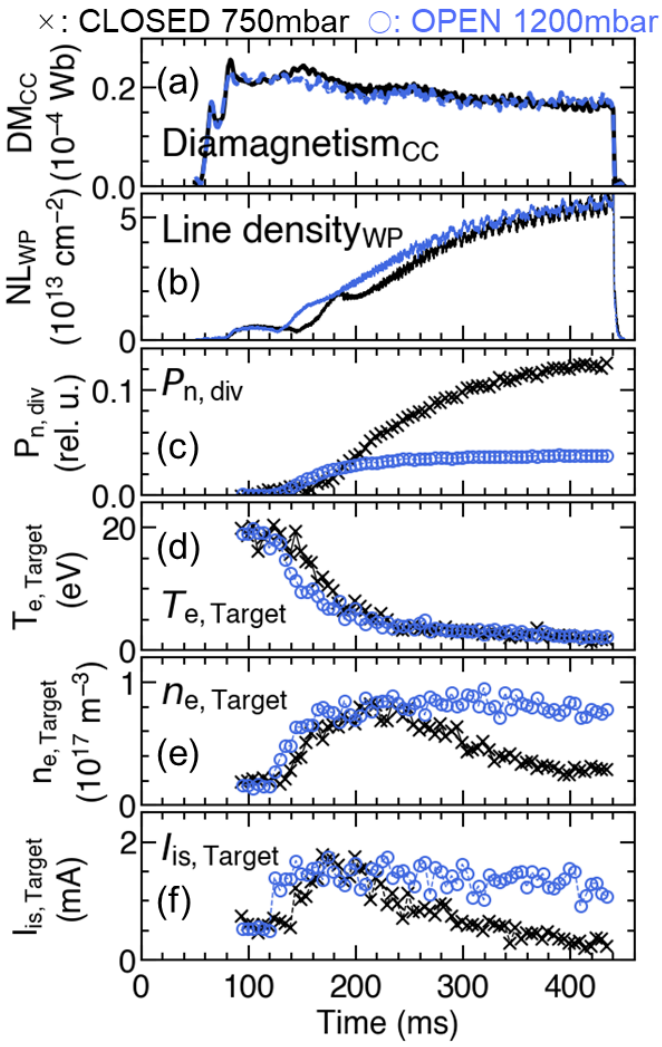

Figure 3.2.1 Time evolution of (a)DM_{CC}, (b)NL_{WP}, (c)P_n, (d)T_e, (e)n_e, and (f)I_{is}. The T_e, n_e, and I_{is} were measured by a Langmuir probe #1 installed near the corner of the V-shaped target. Black ×: with the exhaust door closed and blue ○: with the door open.

Next, spatial characteristics of plasma in the D-module are focused on. Spatial distributions of T_e, n_e, and I_{is} toward Z axis measured by the LPs #1-5, #17 and #18 when T_e at the LP #1 is ~5 eV are shown in Figures 3.2.2(a), (b) and (c). The distributions of T_e, n_e, and I_{is} with the door open are almost the same as those with the door closed. The same set of distributions as Figs. 3.2.2(a)-(c) measured when T_e at the LP #1 is ~2 eV are shown in Figures 3.2.2(d), (e) and (f). With the door open and closed, T_e distribution is almost the same. Near the inlet of the D-module where the LPs #17 and 18 are installed, distributions of n_e, and I_{is} with the door open are also almost the same as those with the door closed. On the other hand, near the target where the LPs #1-5 are installed,

n_e, and I_{is} with the door open were higher than those with the door closed. Toward Z axis, difference in n_e, and I_{is} between the cases with the door open and closed are confirmed near the target plate. Then the distributions near the target along Y axis which is perpendicular to the Z axis are focused on. The same set of distributions along Y axis near the corner measured by the LPs #2 and #6-9 when T_e at the LP #1 is ~5 eV are shown in Figures 3.2.3(a), (b) and (c). The same set measured when when T_e at the LP #1 is ~2 eV are also shown in Figures 3.2.3(d), (e) and (f). When T_e at the LP #1 is ~5 eV, the distributions along Y axis with the door open are almost the same as those with the door closed. When the T_e at the LP #1 is ~2 eV, T_e distribution along Y axis is almost the same in the both cases. On the other hand, n_e, and I_{is} with the door open are higher than those with the door closed. When T_e at the LP #1 decreases from ~5 eV to ~2 eV, n_e, and I_{is} at the all positions of the LPs #2 and #6-9 with the door closed decreases but those with the door open does not change much. Considering the above distributions toward Z and along Y axis, the plasma parameters near the inlet of the D-module are almost the same in the cases with the door open and closed but there is a clear difference in plasma detachment near the V-shaped target due to the neutral pumping.

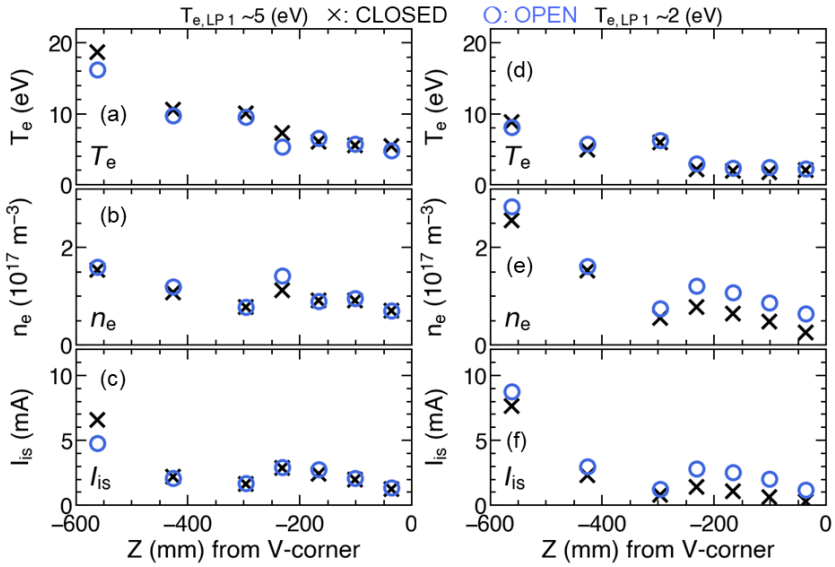

Figure 3.2.2 Spatial distributions of (a)T_e, (b)n_e and (c) I_{is} measured by the LPs #1-5, #17 and #18 when T_e at the LP #1 is ~5 eV, and distributions of (a)T_e, (b)n_e and (c) I_{is} measured when the T_e is ~2 eV. Black ×: with the exhaust door closed and blue ○: with the door open.

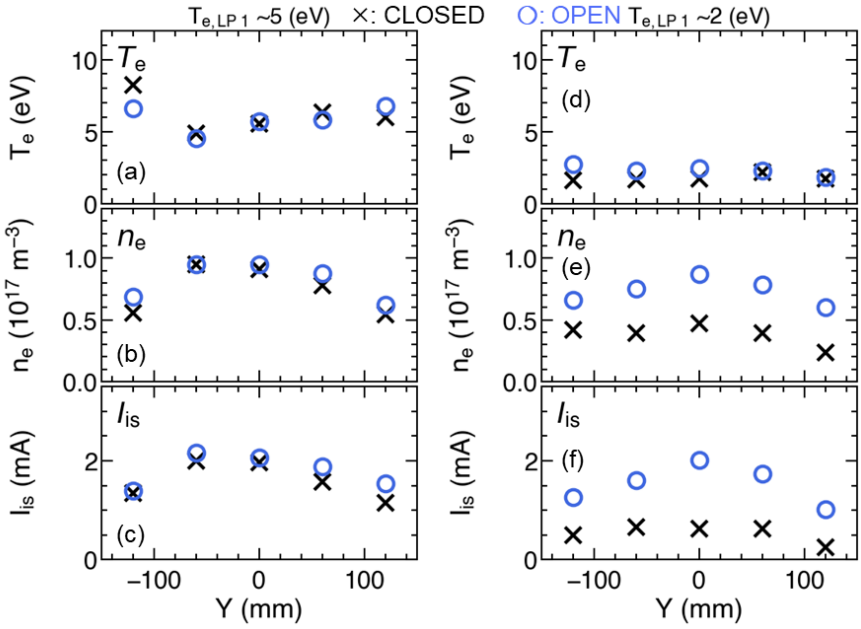

Figure 3.2.3 Spatial distributions of (a)T_e, (b)n_e and (c) I_{is} measured by the LPs #2 and #6-9 when T_e at the LP #1 is ~5 eV, and distributions of (a)T_e, (b)n_e and (c) I_{is} measured when the T_e is ~2 eV. Black ×: with the exhaust door closed and blue ○: with the door open.

3.2.2 Details of the phenomena near the V-shaped target

In the last subsection, a clear difference in plasma has been confirmed near the target plate due to the effect of the pump. Now we study the detail of phenomena near the V-shaped target in the D-module. The plenum pressure was varied in discharges to change T_e and to study T_e dependence of plasma. With the door closed, the additional H_2 gas was supplied at the plenum pressure of 200, 400, 600, 750 mbar. With the door open, the plenum pressures were 400, 800, 1000 and 1200 mbar. The beginning time and duration of the opening of the piezoelectric valve in all discharges were the same. The dependence of I_{is}, n_e, $H\alpha$ line intensity ($I_{H\alpha}$), $H\beta$ line intensity ($I_{H\beta}$) and P_n on T_e is shown in Figures 3.2.4(a) to (e). These data were measured from t ≥ ~100 ms. The T_e, I_{is} and n_e were measured by the LP near the corner (#1). The Balmer line spectra were measured by a spectrometer USB2000+ which has a view line near the center of the V-shaped target as shown in Figure 2.1.2. With the door closed, a clear rollover of I_{is} and n_e is observed with decrease in T_e. With decrease in T_e and n_e, $I_{H\beta}$ decreased but $I_{H\alpha}$ increased. This tendency of Balmer line intensities suggests the promotion of DA-MAR process [41] as shown in Table 1 in subsection 1.4. The DA-MAR process consists of the DA and MN reactions. As a result of the MN reaction, an excited hydrogen atom with the principal quantum number n = 2 or 3 is produced and the one with n = 3 emits $H\alpha$ line. In the both of the cases with the door closed and open, I_{is} has a peak at T_e = ~10 eV and n_e has a peak at T_e = ~5 eV. Before each rollover, T_e dependence of I_{is} and n_e is almost the same in the both cases. After the rollover, on the other hand, I_{is} and n_e with the door open are higher than those with the door closed in almost the same T_e range. This tendency seems that T_e dependence of I_{is} and n_e bifurcates when T_e decreases due to the pump, suggesting that MAR processes become difficult to occur even though T_e decreases to a few eV when the exhaust door is open. In this T_e range where the dependences are different, P_n with the door open is lower than half of that with the door closed, indicating that the H_2 density in the D-module with the door open is lower. When T_e is around 3 eV, $I_{H\alpha}$ with the door open is lower than that with the door closed, suggesting that the MN reaction rate with the door open is lower.

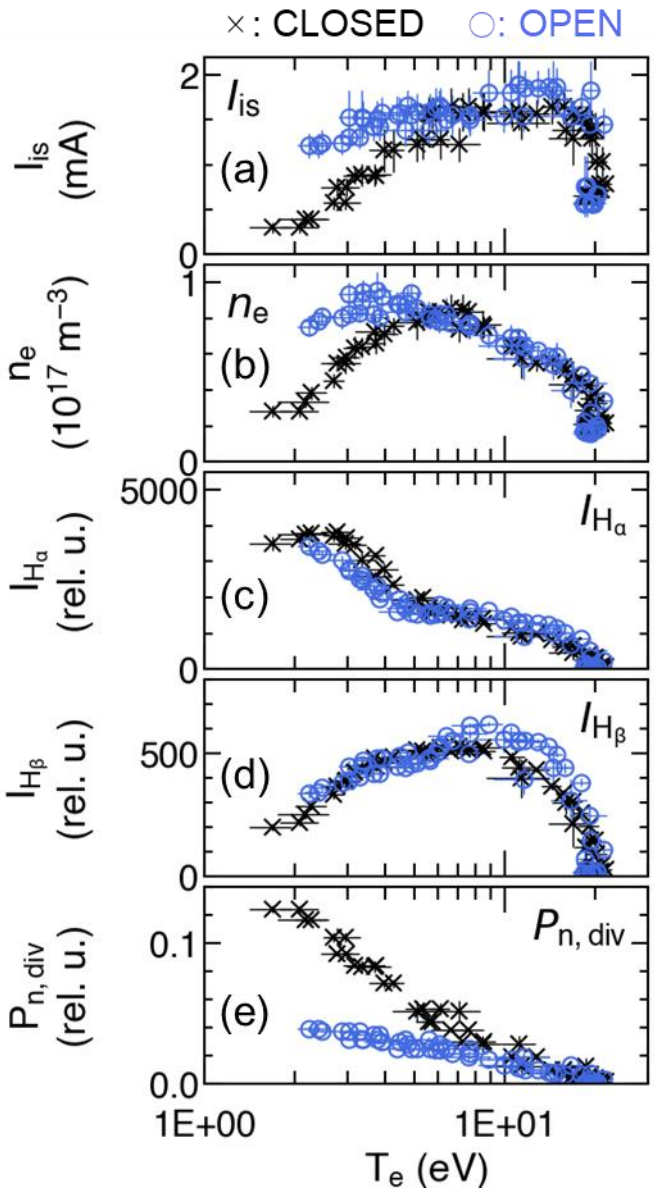

Figure 3.2.4 T_e dependence of (a)I_{is}, (b)n_e, (c)$I_{H\alpha}$, (d)H_β and (e)Pn. Black ×: with the exhaust door closed and blue ○: with the door open.

3.2.3 Discussion

Next, the reason why the MAR processes near the corner of the V-shaped target are difficult to occur with the pump are discussed. In the same T_e range, as written with the colored letters in Table 2, three factors can be considered to cause the difference in MAR reaction rate between the cases with the door open and closed: 1)the vibrational and rotational states of H_2, 2)the density of H_2 (n_{H2}) and 3)the temperature of H^+ (T_i). The vibrational and rotational states and density of H_2 affect the reaction rates of the DA, CNV and MIC reactions. The rate coefficients and the reaction rates of the MN and CNV reactions depend on T_i.

Table 2. Reaction processes in MAR and three factors (colored) which can be considered to cause the difference in MAR reaction rate when T_e is the same.

• DA-MAR	・DA	$H_2(v) + e \rightarrow H^- + H$
	・MN	$H^- + H^+ \rightarrow H + H^*(n = 2,3)$
• IC-MAR	・IC	$H_2(v) + H^+ \rightarrow H_2^+(v) + H$
	・DR2	$H_2^+(v) + e \rightarrow H + H^*$
• MIC-MAR	・IC	$H_2(v) + H^+ \rightarrow H_2^+(v) + H$
	・MIC	$H_2(v) + H_2^+(v) \rightarrow H_3^+(v) + H$
	・DR3	$H_3^+(v) + e \rightarrow 3H, H_2(v) + H^*$

3.2.3.1 Effect of rovibrational states and density of hydrogen molecules

First, the vibrational temperature (T_{vib}) and rotational temperature (T_{rot}) of H_2 were evaluated from Fulcher-α band spectra [49-50] measured by a spectrometer SR-500i which has a view line near the corner of the target as shown in Figure 2.1.2 and from T_e measured by the LP #1. Figure 3.2.5 shows the T_e dependence of (a)T_{vib} and (b)T_{rot} when T_e was lower than ~6 eV. The error bars were evaluated from the fitting error of relative population densities of $d^3\Pi_u^-$ state of hydrogen molecules at various rovibrational states. In the same T_e range, T_{vib} with the door open is almost the same as that with the door closed. As for T_{rot}, there was a variation in measurement of this

experiment. In order to improve the precision by integrating the spectra and to check the reproducibility, another experiment was conducted in the same plasma condition. Unfortunately, the total neutral pressure in the D-module could not be measured due to a trouble with the ASDEX type gauge but T_{vib} and T_{rot} was evaluated with better precision. Figure 3.2.6 shows the result of the new experiment. With decrease in T_e near the corner, both I_{is} and n_e show tendencies similar to those in Fig. 3.2.4. As a result of more precise experiment, it turns out that there is not clear difference in value of T_{rot} between the case with the exhaust door open and closed. These tendency of T_{vib} and T_{rot} indicates that the rate coefficients of the DA reaction (k_{DA}) in the both cases are almost the same.

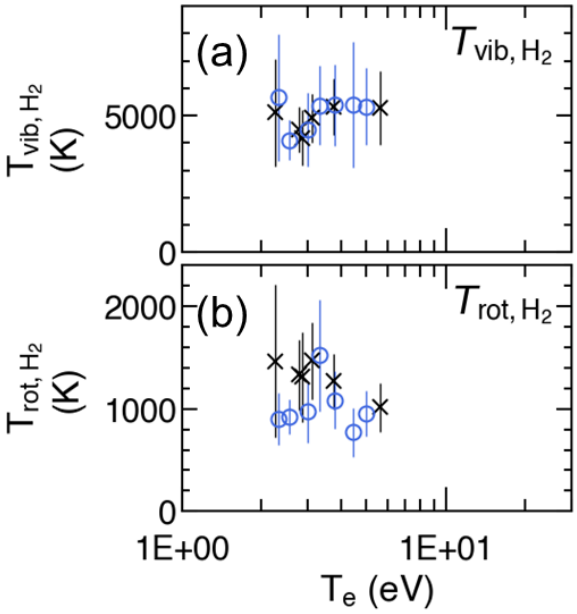

Figure 3.2.5 T_e dependence of (a)T_{vib} and (b)T_{rot} of H_2 evaluated from Fulcher-α band spectra. Black ×: with the exhaust door closed and blue ○: with the door open.

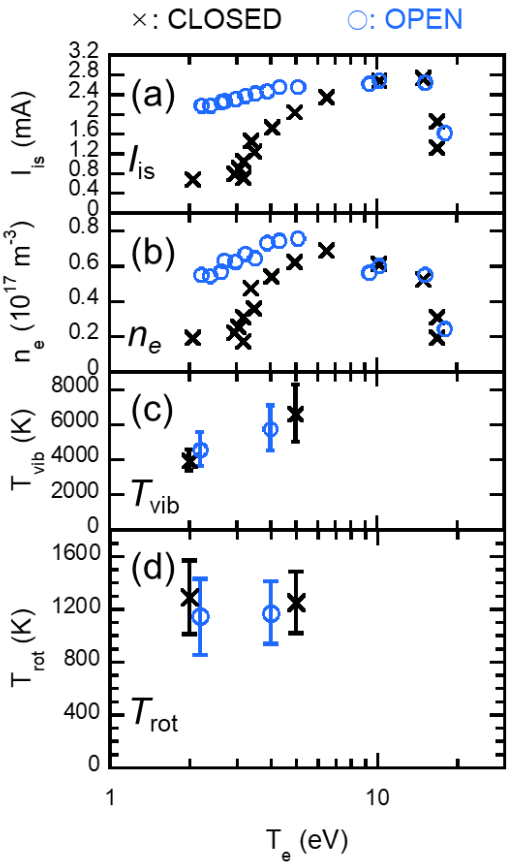

Figure 3.2.6 Results of newer experiment with the same plasma condition and with more precision of T_{vib} and T_{rot} measurement. T_e dependence of (a)I_{is}, (b)n_e, (c) T_{vib}, and (d) T_{rot}. Black ×: with the exhaust door closed and blue ○: with the door open.

To analyze the MAR reaction rates, next n_{H2} and the product of n_{H2} and n_e ($n_{H2}\times n_e$) are considered. When the values of T_e, T_{vib} and T_{rot} are constants, the intensity of Fulcher-α band spectra lines is proportional to $n_{H2}\times n_e$. Since T_{vib} and T_{rot} in both of the cases with the door closed and open are almost the same at the same T_e, the intensity can be used as an indicator of $n_{H2}\times n_e$. Figure 3.2.7 shows Fulcher-α band spectra with the door open and closed. In the both cases, T_e is ~2 eV. The intensity of Q1 branch ($v = v' = 0$) of the spectra (I_{Q1}) is highest in both cases. Then, Figure 3.2.8 shows the T_e dependence of (a) I_{Q1} and (b)I_{Q1} normalized by n_e (I_{Q1}/n_e) which is proportional to n_{H2} in the same range of T_e, T_{vib} and T_{rot}. These T_e and n_e were measured by the LP #1. In the both cases, I_{Q1} is almost the same at the same T_e, indicating that $n_{H2}\times n_e$ is also almost the same with the door open and closed. Combining the above results about k_{DA} and $n_{H2}\times n_e$, the DA reaction rate with the door open and closed can be considered to be almost the same. When T_e is higher than ~5 eV, I_{Q1}/n_e with the door open and closed are almost the same. On the other hand, when T_e is lower than ~5 eV, I_{Q1}/n_e with the door open is lower than that with the door closed,

indicating that n_{H2} near the corner of the V-shaped target with the door open is lower. When T_e is around 3 eV, I_{Q1}/n_e indicates that I_{Q1}/n_e near the corner with the door open is about the half of that with the door closed. It should be noted that with the door open, decrease in T_e occurs with lower H_2 density.

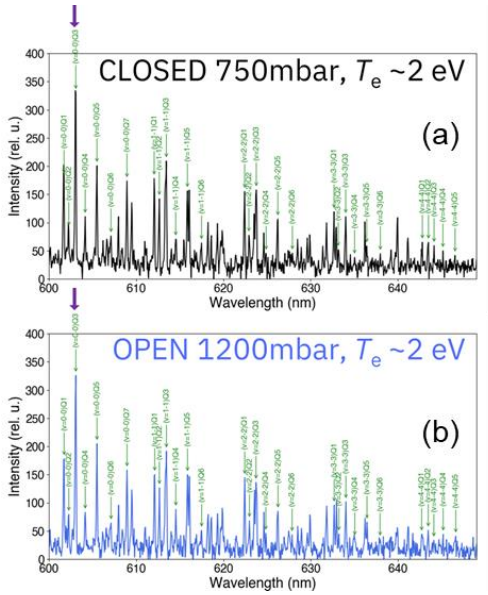

Figure 3.2.7 Fulcher-α band spectra measured when T_e near the corner of the V-shaped target was ~2 eV. (a): with the door closed and (b): open.

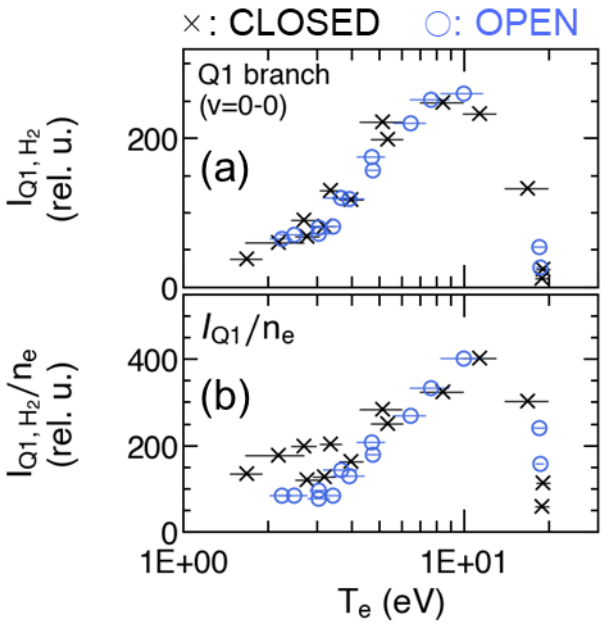

Figure 3.2.8 T_e dependence of (a)intensity of the Q1 branch (v = v' = 0) of Fulcher-α band spectra and (b)the Q1 branch intensity normalized by n_e measured by the LP #1. Black ×: with the exhaust door closed and blue ○: with the door open.

3.2.3.2 Effect of ion temperature

Next, the effect of T_i is discussed. The rate coefficient of MN and IC processes depends on T_i. Unfortunately, there is no direct T_i diagnostic in the D-module and the only information on T_i was that $T_{i\|}$ without the additional hydrogen gas around 100 eV, which was measured by ELIEA in the same condition of plasma discharge except for that the position of D-module was under the axis in order to enable ELIEA measurement. Then, we assume the upper limit of T_i was ~100 eV. Figure 3.2.9 shows the T_i dependence of the rate coefficients of the MN and the IC processes calculated by using the cross sections in Ref. [24] and T_{vib} = 5000 K in the range of $T_i \leq 120$ eV. In most region of the T_i range, if T_i with the door open was higher than T_i with the door closed, the rate coefficients of the MN and IC reactions with the door open became higher than those with the door closed and reaction rates with the door open would become higher. This is not consistent with the experimental results. Thus, it is considered that T_i with the door open was lower than T_i with the door closed at the same T_e to reduce the MAR rate coefficient,

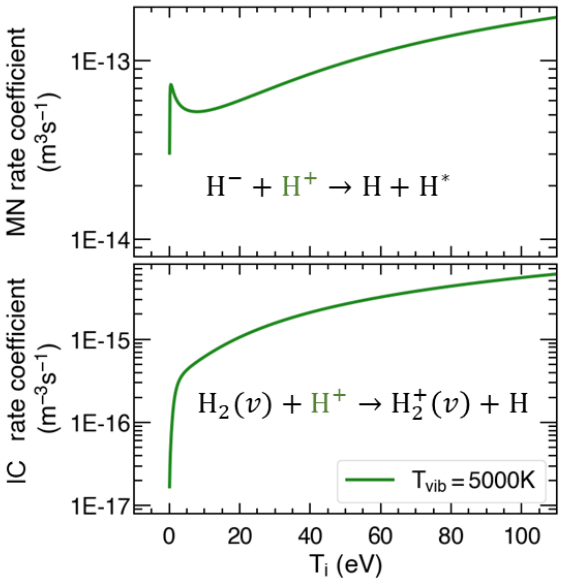

Figure 3.2.9 T_i dependence rate coefficients of (a) MN and (b) IC reactions calculated by using cross sections in Ref. [24] and T_{vib} = 5000 K.

Then, whether T_i with the door open could be lower than T_i with the door closed at the same T_e is discussed. Possible processes which decrease T_i are charge-exchange and elastic scattering between ions and neutrals. Figure 3.2.10 shows ion energy dependence of cross sections of charge-exchange and elastic collision process between ion and neutral atoms. Each cross section is still large when the ion energy is low. As for ion mean free path (MFP) of charge-exchange process between ions and neutral hydrogen atoms, MFP with T_i ~50 eV, stational atoms and neutral pressure of ~10 Pa is evaluated to be ~3 mm. The pressure of ~10 Pa is the past result with H_2 plenum pressure of 800 mbar and with the door closed [43]. Since the MFP is much shorter than the length of the D-module (~700 mm), ions can lose energy through charge-exchange process with statinal atoms before going out of the exhaust door. To reduce T_i, low temperature atom is effective. Considering these results and the experimental condition where the amount of supplied H_2 gas with the door open was more than that with the door closed, it is expected that ions with the door open could lose more energy due to low temperature atom than that with the door closed.

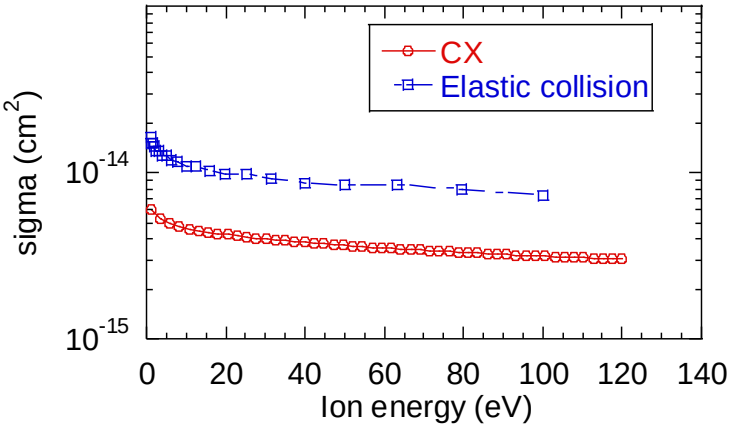

Figure 3.2.10 Ion energy dependence of cross section of charge-exchange (CX) and elastic collision process between ion and neutral atoms. Data are taken from Ref. [51].

3.2.4 Summary

In this study, neutral particle effect on plasma detachment is investigated by changing the balance between gas puff and pump, focusing on that neutral parameters such as temperature, density and quantum states are affected by the gas puff and pump. Characteristics of hydrogen gas supply and exhaust were changed by adjusting the exhaust door of the D-module and the amount of gas supply. As a result, in the upstream of the V-shaped target, the same condition of plasma was sustained regardless of the balance between the gas puff and pump. On the other hand, near the target, degree of plasma detachment changed with the balance. These results clarified that the reaction rate of MAR leading to plasma detachment changes with the balance between gas puff and pump. Difference in three factors can be considered to change the reaction rate: (i) vibrational and rotational states of H_2, (ii) H_2 density and (iii) T_i. Vibrational and rotational temperatures of H_2 evaluated from Fulcher-α spectra did not change with the gas supply and exhaust characteristics but H_2 density with the exhaust door open evaluated by dividing the Fulcher-α band spectra intensity by n_e was lower. Also, it was shown that much gas supply with strong pump promotes gas replacement in the D-module and it makes T_e to decrease with lower H_2 density. In addition, effect of T_i was considered by using parameters such as rate coefficients which depend on T_i and it is suggested that the MAR reaction rate changed due to changes in H_2 density and T_i caused by gas puff and pump.

Chapter 4

Conclusion

In order to reduce heat and particle load on divertor plate in magnetic confinement fusion reactors, detached divertor operation is considered to be an effective method and understanding of physical mechanism of plasma detachment is needed. Electron temperature (T_e), ion temperature (T_i) and neutral parameters including temperature, density and quantum states of atoms and molecules are important for plasma detachment. In tokamaks, T_i of divertor plasma during detachment has not been measured due to difficulty in measuring in the condition with high neutral pressure, low temperature and density plasma. In order to clarify effects of T_i on plasma detachment, measuring spatial distribution and temporal behavior of T_i is important. Therefore, development of simple measuring method of T_i is needed. In addition, in contrast to the deeper database of effect of neutral parameters on individual atomic and molecular processes related to the plasma detachment, experimental database of effect of the neutral parameters such as temperature, density and quantum state on plasma detachment is not sufficient. For instance, contribution of molecular activated recombination (MAR) to plasma detachment in tokamaks is controversial. The aim of this thesis is I) to develop a simple measuring method of T_i and II) to investigate neutral particle effect on plasma detachment.

With respect to I) T_i measuring method, the objective of this thesis is to develop an evaluation method of ion temperature parallel to the magnetic field ($T_{i||}$) by using a Langmuir probe (LP), focusing on the contribution of the product of $T_{i||}$ and ion polytropic index (γ) to the ion saturation current measured by the LP. LPs have advantages of simple structure and low cost. In order to develop the evaluating method of $T_{i||}$ by using an LP, an experiment was conducted utilizing the high $T_{i||}$ plasma in the end region of the GAMMA 10/PDX tandem mirror and wide range $T_{i||}$ regime. In this experiment, characteristics of $\gamma T_{i||}$ evaluated by using an LP when $T_{i||}$ was varied were investigated. The evaluated $\gamma T_{i||}$ was compared with $T_{i||}$ measured by an ion energy analyzer. The value of $T_{i||}$ of the end-loss plasma was varied by using ICRF heating of the central plasma and additional gas puff in the central cell. Applying the ICRF heating, $T_{i||}$ measured by the analyzer ($T_{i||,IEA}$) was increased and $\gamma T_{i||}$ evaluated by the LP ($\gamma T_{i||,LP}$) was decreased. When the additional gas was supplied in addition to the ICRF heating, both $T_{i||,IEA}$ and $\gamma T_{i||,LP}$ were decreased. The value

of γ was evaluated as the ratio of $\gamma T_{i\parallel,LP}$ and $T_{i\parallel,IEA}$. The results experimentally suggest that without changes in the ion-ion collisionality and ion-neutral collisionality, γ decreases with increase in $T_{i\parallel}$ due to a high ion temperature component. To improve quantitativity in evaluation of $T_{i\parallel}$ using a Langmuir probe, expansion of database on the value and characteristics of γ by experiments and kinetic simulation is considered to be an effective method. This is a future work.

With respect to II) neutral particle effect on plasma detachment, the objective of thesis is to change neutral states by neutral particle replacement using gas injection and particle exhaust and to investigate the effect of neutral particle states on plasma detachment. Characteristics of hydrogen gas supply and exhaust were changed by using the gas exhaust door and changing the amount of gas supply in the divertor simulation region of GAMMA 10/PDX. Though upstream plasma of the target plate installed in the divertor simulation module was sustained regardless of the balance between the gas puff and pump, degree of plasma detachment near the target plate with the door open was lower than that with the door closed. The detailed analysis of these results have clarified that with the exhaust door open and supplying the gas more, despite the decrease in T_e, reaction rate of MAR leading to plasma detachment decreases despite the decrease in T_e. Difference in three factors which affect the reaction rate was investigated: (i) vibrational and rotational states of H_2, (ii) H_2 density and (iii) T_i. Vibrational and rotational temperatures of H_2 evaluated from Fulcher-α spectra did not change with the gas supply and exhaust characteristics but H_2 density with the additional pump evaluated by the ratio of the Fulcher-α band spectra intensity to n_e was lower with the exhaust door open. This results also show that T_e with the exhaust door open decreases at lower H_2 density than that with the door closed. In addition, effect of T_i was considered by using parameters such as rate coefficients which depend on T_i and ion mean free path of charge-exchange reaction. It is suggested that T_i and the rate coefficient with the exhaust door open may be lower than that with the door closed and it is expected that T_i became lower due to low temperature atoms resulting from the gas replacement. These results suggest that the MAR reaction rate became low due to low H_2 density and low T_i caused by changing the balance between gas puff and pump.

References

[1] R. Aymar *et al*., Plasma Phys. Control. Fusion **44** (2002) 519.

[2] C.S. Pitcher *et al*., Plasma Phys. Control. Fusion **39** (1997) 779.

[3] G. Federici *et al*., Fusion Eng. Des. **109–111** (2016) 1464.

[4] K. Tobita *et al*., Fusion Eng. Des. **136** (2018) 1024.

[5] A. Loarte *et al*., Nucl. Fusion **47** (2007) S203.

[6] G.F. Matthews, J. Nucl. Mater. **220–222** (1995) 104.

[7] S.I. Krasheninnikov *et al*., Phys. Plasmas **23** (2016) 055602.

[8] S.I. Krasheninnikov *et al*., J. Plasma Phys. **83** (2017) 155830501.

[9] A.W. Leonard, Plasma Phys. Control. Fusion **60** (2018) 044001.

[10] J. Boedo *et al*., Plasma Phys. Control. Fusion **60** (2018) 044008.

[11] M. Kocˇan *et al*., J. Nucl. Mater. **415** (2011) S1133.

[12] R.A. Pitts *et al*., Proc. 30th EPS Conf. on Control. Fusion and Plasma Phys. (St Petersburg) 2003 vol 27A (ECA) p 2.84.

[13] R.A. Pitts *et al*., Rev. Sci. Instrum. **74** (2003) 4644.

[14] N. Asakura *et al*., Nucl. Fusion **39** (1999) 1983.

[15] N. Asakura *et al*., Rev. Sci. Instrum. **66** (1995) 5428.

[16] J.A. Boedo *et al*., Phys. Plasmas **23** (2016) 092506.

[17] B. Coppi *et al*., Proc. 17th International Fusion Energy Conference, IAEA-F1-CN-TH3/7 (1998).

[18] D. Brunner *et al*., Plasma Phys. Control. Fusion **55** (2013) 095010.

[19] D. Brunner *et al*., Rev. Sci. Instrum. **84** (2013) 053507.

[20] S. Elmore *et al*., Plasma Phys. Control. Fusion **54** (2012) 065001.

[21] S. Elmore *et al*., J. Nucl. Mater. **438** (2013) S1212.

[22] N. Ezumi *et al*., J. Nucl. Mater. **241-243** (1997) 349.

[23] R.K. Janev *et al*., *Elementary Processes in Hydrogen–Helium Plasmas* Springer-Verlag, Berlin-Heidelberg (1987).

[24] R.K. Janev, *et al*., *Collision processes in low-temperature hydrogen plasmas* FZ-Juelich Report, 4105 (2003).

[25] R.K. Janev, *et al*., J. Nucl. Mater. **121** (1984) 10.

[26] S.I. Krasheninnikov *et al*., Phys. Lett. A **214** (1996) 285.
[27] A.Yu. Pigarov *et al*., Phys. Lett. A **222** (1996) 251.
[28] N. Ohno *et al*., Phys. Rev. Lett. **81** (1998) 818.
[29] J. Horacek *Rate Coefficients for Low Energy Electron Dissociative Attachment to Molecular Hydrogen* NIFS-DATA.
[30] C. Kurz *et al*., Plasma Phys. Control. Fusion **39** (1997) 963.
[31] G.M. McCracken et al., Nucl. Fusion **38** (1998) 619.
[32] K. Fujimoto *et al*., Plasma Fusion Res. **4** (2009) 025.
[33] U. Wenzel *et al*., Nucl. Fusion **39** (1999) 873.
[34] J.L. Terry *et al*., Phys. Plasmas **5** (1998) 1759.
[35] H. Kubo *et al*., J. Nucl. Mater. **337-339** (2005) 161.
[36] U. Fantz *et al*., J. Nucl. Mater. **290-293** (2001) 367.
[37] N. Ohno, Plasma Phys. Control. Fusion **59** (2017) 034007.
[38] T. Imai *et al*., J. Plasma Fusion Res. **87** (2011) 752.
[39] Y. Nakashima *et al*., Nucl. Fusion **57** (2017) 116033.
[40] Y. Nakashima *et al*., Fusion. Sci. Technol. **68** (2015) 28.
[41] M. Sakamoto *et al*., Nucl. Mater. Energy **12** (2017) 1004.
[42] A. Terakado et al., AIP Conf. Proc. **1771** (2016) 050008.
[43] K. Nojiri et al., AIP Conf. Proc. **1771** (2016) 060008.
[44] Y. Nakashima *et al*., Vacuum **41** (1990) 1561.
[45] P.C. Stangeby, *The Plasma Boundary of Magnetic Fusion Devices* (IOP, Bristol, 2000).
[46] E. Zawaideh *et al*., Phys. Fluids **29** (1986) 463.
[47] K.-U. Riemann, J. Phys. D: Appl. Phys. **24** (1991) 493.
[48] B. Lin *et al*., Phys. Plasmas **23** (2016) 083508.
[49] B. Xiao et al., Plasma Phys. Control. Fusion **46** (2004) 653.
[50] A. Terakado et al., Plasma Fusion Res. **13** (2018) 3402096.
[51] IAEA ALADDIN database, https://www-amdis.iaea.org/ALADDIN

Acknowledgments

The author would like to express his sincere gratitude to Prof. Mizuki SAKAMOTO for significant suggestions and helpfull discussions in the course of the present day. The author especially thanks to Dr. Naomichi EZUMI for important discussions and helpful advices in the course of the present study. The author is grateful to Prof. Yousuke NAKASHIMA for helpful advices on the present day. The author is also grateful to Dr. Ryutaro MINAMI for helpful comments.

The author would like to thank Dr. Satoshi TOGO and Dr. Takaaki IIJIMA for helpful discussions and joyful private communications.

The author thanks Mr. (Dr. in near future) Akihiro TERAKADO for studying, doing experiments, discussing and talking together for the five years in Plasma Research Center.

The author wishes to write down individual name of other members who have helped the author but paper is limited. The author wishes to thank them very much.

For the long year support, the author thanks his family.

Finally, the author would like to thanks you.